3-19-2008

Analysis of Capillary Forces in Electrowetting and Precision Self Assembly

Vivek Ramadoss
University of South Florida

Analysis of Capillary Forces in Electrowetting and Precision Self Assembly

by

Vivek Ramadoss

A thesis submitted in partial fulfillment
of the requirements for the degree of
Master of Science in Mechanical Engineering
Department of Mechanical Engineering
College of Engineering
University of South Florida

Major Professor: Nathan Crane, Ph.D.
Craig Lusk, Ph.D.
Wilfrido Moreno, Ph.D.

Date of Approval:
March 19, 2008

Keywords: Preload Force, Surface Evolver, Repeatability, Alignment Constraint, Dielectric Layer

DEDICATION

To my Parents

ACKNOWLEDGEMENTS

I wish to acknowledge the gracious support of many people for their contributions towards this work both directly and indirectly. Firstly, I thank my advisor Dr. Nathan Crane who patiently guided me through all phases of this work. He is a true role model, and a best professor I have ever seen. The time and effort of Dr. Craig P. Lusk and Dr. Wilfrido Moreno as committee members are greatly appreciated.

I would like to thank my brother, Balaji Ramadoss for his support, suggestions and invaluable encouragement that have always made me a better man and have indirectly prepared me to tackle challenges that I came across. Without my parents support and encouragement, I never would have made it this far.

Additionally, I would like to thank all my friends and my friends especially from the research group Pradeep Mishra, Jeff Murray, and Jairo Chimento for having always motivated and accompanied me throughout the challenges of research. Without their help, this thesis would have been much more difficult.

This work has been supported in part through the University of South Florida Research Education Initiative Program under grant number FMMD04.

TABLE OF CONTENTS

LIST OF TABLES

LIST OF FIGURES

LIST OF EQUATIONS

Analysis of Capillary Forces in Electrowetting and Precision Self Assembly

Vivek Ramadoss

ABSTRACT

Developments in micro and nano technology have great potential in many applications. Two applications that will be addressed in this work are self assembly of microdevices and Electrowetting in microfluidics. Capillary forces are the most critical factor in both of these techniques and need proper characterization. This thesis describes a detailed study of these forces and explains how they were utilized as an effective source of drive in high end applications.

Self assembly is a promising alternative to conventional pick and place robotic assembly of micro components. Its benefits include parallel integration of parts with low equipment costs. Various approaches to self assembly have been demonstrated, yet demanding applications like assembly of micro-optical devices require increased positioning accuracy. This thesis proposes a new method for design of self assembly bonds that addresses this need. Current methods have zero force at the desired assembly position and low stiffness. The proposed method uses a substrate assembly feature to provide a high accuracy alignment guide to the part. The capillary bond region of the part and substrate are then modified to create a non-zero positioning force to maintain the part in the desired assembly position. Capillary force models show that this force aligns the part to the substrate assembly feature and reduces the sensitivity of part position to

process variation. Thus, the new configuration analyzed proves substantial improvement in positioning accuracy of capillary self assembly. Guidelines are proposed for the design of an effective assembly bond using this new approach.

Electrowetting is another application that has been successfully demonstrated as a means of drop manipulations in digital micro-fluidic devices. These demonstrations show that electrowetting actuation holds great promise, but there are also reports of erratic behavior and system degradation. While a method for electrowetting force measurement to track the degradation of the electrowetting response was demonstrated, this thesis analyzes some adverse effects in the electrowetting response due to variations during measurement of electrowetting forces, specially the variation of volume, the tilt in the part considered for measurements, and defective layer response.

CHAPTER 1 INTRODUCTION

1.1 Thesis Statement

The thesis will address the applied capillary forces in self assembly and electrowetting applications. Modeling methods are used to investigate the impact of variation on the reliability of two different systems based on capillary forces. The first system is a fluidic self assembly process. This work will show how the forces can be optimized in the process of self assembly to meet precision assembly standards at the micro scale. The second system to be modeled is an electrowetting force measurement system. A nanoindenter has been adapted for measurement of the electrowetting forces under an applied voltage. This thesis models the forces induced by electrowetting and analyses their sensitivity to variation to determine the usefulness of these methods in characterizing the substrate's electrical and surface properties.

This chapter will review the background, overall concept, and critical factors involved in each application. For improved use of the capillary force, a novel design is proposed and analyzed for accuracy.

1.2 Background

1.2.1 Self Assembly

Complex systems available in the market today are made by integration and interconnection of various components to create an object that performs the required functions. Assembly is the key manufacturing process of many such integrated systems. In macro-scale applications, assembly requirements have relied on robotic pick and place assembly lines to integrate and interconnect components at all complexities. The evolution of micro-manufacturing has led to components to the micro & nano scale with various functionalities integrated onto a single device.

In the pick and place methods, a major concern at smaller size scales is the sticking effect due to the attraction forces such as the Van der Waals and electrostatic forces. Also, pick and place methods lose their advantage when assembling large numbers of micro parts of diverse sizes due to lack of a parallel assembly process.

To address these limitations, technologies such as micromanipulator based assembly [1], and wafer to wafer devices transfer [2] have been developed in order to integrate micro components. Special micromanipulators were designed to aid micro assembly requirements, yet these manipulators proved to be less efficient due to the inline assembly approach. These difficulties necessitated the need for a novel assembly technique thus leading to the concept of self assembly.

Self assembly is a promising alternative technique to conventional assembly methods. Its advantages include a parallel assembly approach, 3D integration compatibility, cost effectiveness, and feasibility in the assembly of components of different sizes and characteristics.

Self assembly concepts originated in organic chemistry at the molecular scale. Recent works in the field have proven that this technique has potential in the assembly of components on the micro and nano scale. This technique offers simplicity and economy in processes that work on components which are too small or too numerous to be manipulated by other means.

Self assembly can be defined as a process where a system of disordered components forms an organized structure without the necessity of grasping and placing the components. An external input is needed to obtain a series of random interactions usually through agitation. A driving force must be created in the system for the system to reach a state of minimum global energy. If parts are to be assembled to a substrate by self assembly, the substrate must be defined with binding sites that create the energy minima. When the substrate is brought into contact with the parts as by immersing in a fluid medium with suspended parts, the parts will bond to the substrate. In such a case, when a substrate is immersed in a medium where the parts are agitated or randomly moved, the parts tend to fill the substrate binding sites. Figure 1 illustrates self assembly through agitation in a fluidic medium.

Self assembly is a process of assembling parts together driven by the minimization of various energies. These include gravitational, magnetic, electrostatic and interfacial energies. Figure 2 shows the energy profile in a generic capillary self assembly system, where the energy of the system as a function of the part position is detailed. The final assembly position is the one with the lowest energy thus demonstrating the concept of energy minimization.

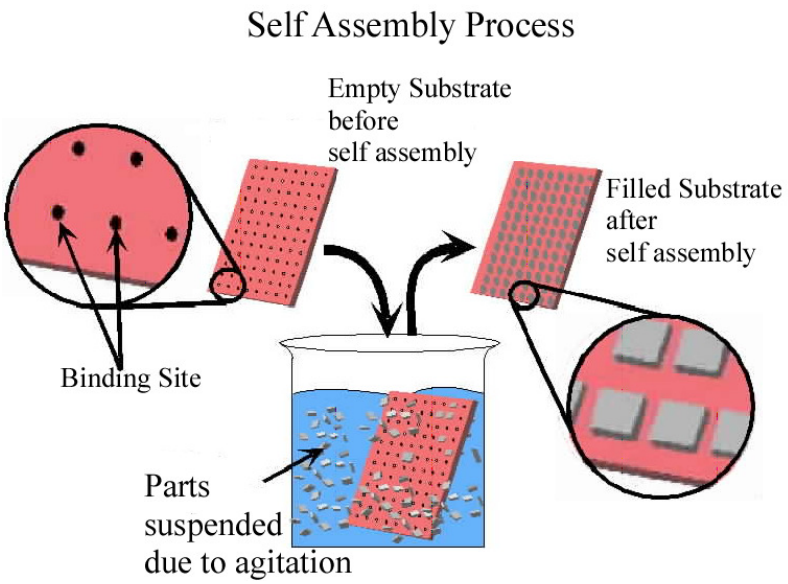

Figure 1 Schematic representation to illustrate a generic self assembly process.

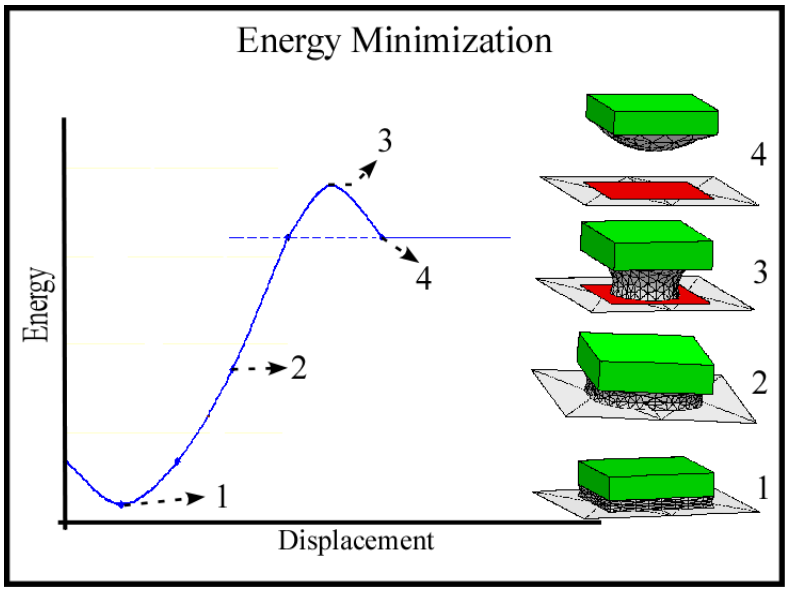

Figure 2 Representation of the system at different positions. The numbered positions start at the assembled position and then move to the disassembled state.

In general, self assembly takes place in an agitated fluidic medium as it facilitates 3D motion and interaction of the components. The advantage of self assembly in the fluidic medium is that it provides a constant supply of parts to the binding sites and removes all the parts from the site that are not bound. Parts that are fully bound are not displaced by the fluid force as their attractive forces are stronger than the agitation forces.

Self assembly in the fluidic medium is usually combined with other techniques of self assembly in [3-5].

1.2.2 Types of Self Assembly

In general there are two types of self assembly: static self assembly & dynamic self assembly [6]. In static self assembly, the system does not require an external force/energy to create the global equilibrium state because it is a position of energy minimum within the system. Static self assembly requires a source of external energy to help the components reach the minimum energy position. Once the components reach their minimum energy position, the energy input may be removed and the system remains stable.

Dynamic self assembly can be applied to a system that attains its equilibrium state when an external force/energy is applied. The applied energy is continuously dissipated in the system to create a minimum energy configuration that only exists while the energy is being dissipated [6].

1.2.3 Self Assembly Forces

There have been numerous energy and force types used to drive the self assembly process. All these sources have different constraints and limitations although every method proves to be effective. Some of the chief methods are described below.

1.2.3.1 Assembly by Capillary Force

Many self assembly techniques rely on the concept of a capillary or surface tension bond. Figure 3 gives a schematic representation of assembly of a part to the binding site by capillary forces.

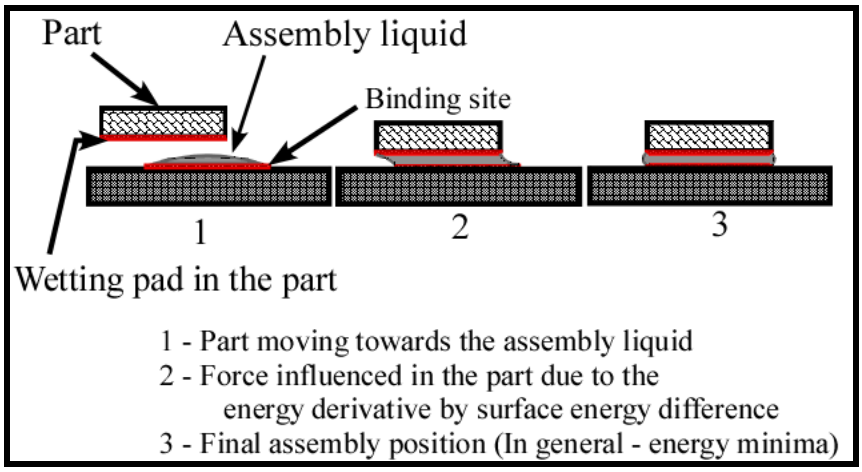

Figure 3 Schematic of assembly by capillary forces.

Capillary forces are very effective due to the fact that the surface tension forces dominate the gravitational forces when the part size is small (<1mm). Hence assembly in such a case is done by the hydrophobic and hydrophilic interactions, reactions due to the difference in the surface energy. Greiner et al. [7] demonstrated a case in which the energy difference was nearly two orders of magnitude. The solid-fluid interface and the solid-assembly liquid interface provide the driving force for assembly. This process of self assembly is our major concern and hence a detailed review on the works done and results obtained using this method is summarized in Chapter 2.

1.2.3.2 Assembly by Electrostatic Force

Although capillary force bonding is an efficient method in self assembly, an alternate source with a longer range of interaction is sometimes favorable. This type of long range interaction in self assembly can be achieved by the electrostatic force that is obtained by the polarization of the micro parts in electric fields. This assembly technique is by the principle of Coulomb's law which states that the attraction or the electrostatic force is inversely proportional to the square of the distance between unlike charges.

Using this approach, attraction towards components can be increased by increasing the electric field intensity.

Tien et al. [8] proposed the technique of micro-fabrication using electrostatic self assembly. The longer range of interactions provided by electrostatic force compared to the hydrophobic or hydrogen-bonding interactions facilitated the proposed method. Overlaps (two parts gets assembled on to a single location) in this assembly technique were eliminated by designing parts with approximately 1:1 aspect ratio. The work detailed convenient methods to generate charged microstructures using a self-assembled monolayer.

1.2.3.3 Assembly by Magnetic Force

Magnetic forces are another possible driving potential for self assembly. By the principle of magnetism, two magnetic surfaces always attract each other provided they belong to opposite poles. When a system is designed in such a way that the site is of the opposite polarity of the part, mere agitation of the system would assemble the part on the assembly location. Yet this method has its own drawback of just being attracted to the site and does not deal with the accuracy in positioning or orientation. This assembly technique is feasible for short range interactions and three-dimensional integration of microstructures.

Shet et al. [9] proposed a simple assembly model using the magnetic field to assemble nano scale semiconductor devices. This process consisted of two assembly steps assisted by the magnetic field. This work also addressed the advantages over other methods including elimination of damage to pre-existing devices on the substrate, elimination of blocking of sites for assembly processes and a clean and dry assembly

environment because the proposed method does not require any fluid medium as in the case of fluidic self assembly process.

Love et al. [10] demonstrated a process of assembly of sub-micron sized metallic rods using magnetic field forces. This demonstration proved that the stabilization and formation of ordered 3D structures can be obtained by the magnetic profile of individual components. Emphasis was made on combining capillary interactions with the magnetic-force fields due to long range interaction requirements. The work addresses the problem of a chain of particles formed as a result of the magnetic dipole interactions and suggested a possible solution for the problem. While there have been few unexpected results in the self assembly of metallic rods, possible suggestions have been detailed and the final bundle of rods assembled is shown to be well ordered, neglecting the dipole interactions as they were comparatively weaker. The advantages of magnetic self assembly include making unnecessary the surface chemistry requirements and that the forces act both in water and air medium thus providing flexibility of the assembly process.

1.2.4 Capillary Self Assembly – Our Concern

Self assembly dictates all the required assembly characteristics in individual components. These characteristics determine the interactions between the components. The main feature of the component is to align and organize among them as they have the ability to move with respect to each other. Once they reach a steady state position, there is a balance between the force of attraction and repulsion.

The focus of our work is the assembly of components by capillary-driven self assembly. Figure 4 shows a part assembled to the binding site on the substrate by

capillary-driven self assembly. This is done by an assembly liquid in between them to drive the assembly process. Here the binding site is defined as the surface that is highly wettable while other surfaces are non-wettable. Hence the assembly liquid and the parts are attracted towards this binding site location when the parts are agitated. .

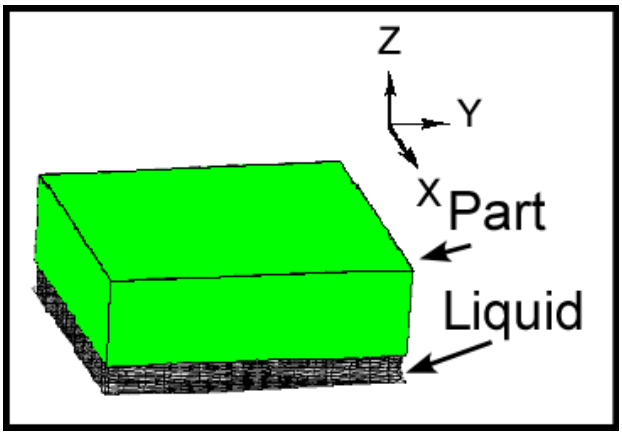

Figure 4 Part assembled on to the binding site with assembly fluid in between them.

1.2.5 Characteristics Influencing Capillary Self Assembly

There are critical factors that can affect the accuracy/effectiveness of the self assembly process. These include binding site shape, surface tension of the fluid, and liquid volume.

1.2.5.1 Surface Tension

Surface tension is the intermolecular attraction force that acts on a liquid medium to change its shape. This force pulls the liquid in all the directions by the neighboring molecules which make the resulting net force to be zero. At the surface of the liquid there is a force of attraction by the molecules deeper inside the liquid although the force is not as intense as the molecules from the neighboring medium. So all liquid molecules are acted on by an inward force of attraction that causes the liquid to be compressed. This is

the reason for the liquid to be compressed together till they reach a minimum surface energy level.

This parameter is responsible for shaping of liquid volumes that plays a major role in self assembly. Surface tension is a property of the fluid and it is often sensitive to parameters such as surface contamination and temperature.

The binding of the liquid to the binding site is by the surface tension force that acts on the liquid, which enables proper alignment of the micro part on the liquid. This liquid being a specific chemical has to be analyzed for its properties and formulated for an efficient approach. There can be two wetting regimes that can be originated due to surface tension (complete wetting and partial wetting). In complete wetting, the liquid phase spreads out on the entire solid phase forming a three layer system (solid, liquid and surrounding medium). In partial wetting technique, the liquid phase stays in a finite region to a form a specific contact angle at a specific contact line [11].

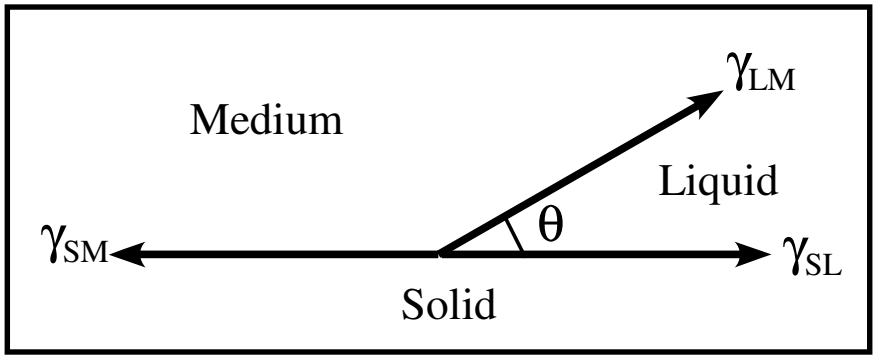

Figure 5 Contact angle (θ) due to surface tensions at interface.

Figure 5 shows an illustration to explain the dependency of contact angle due to surface tensions at the interface of three different medium.

This can be effectively explained with the equation supporting Young condition as

$$\gamma_{SM} = \gamma_{SL} + \gamma_{LM} Cos\theta$$

Equation 1 Young condition to show the contact angle dependence in the surface tension of different medium.

Thus, surface energy of different mediums can be measured by measuring the contact angle made between these mediums. By the implementation of fluidic self assembly, the partial wetting technique can be exploited where the resulting forces due to minimization are due to the driving effect of the fluidic medium [12]. Any change in the surface area due to energy minimization would result in a derivative of work that is proportional to a surface change. This depends on the material that is in contact with the interface. When a surface element is displaced by a small area derivative, the pressure on either side of the interface changes in the medium accompanied by a volume change which also accounts for the change in energy pattern.

Surface tension becomes more important when considering micro scale objects. For this type of assembly using surface tension, a substrate is prepared with surfaces of different surface tensions. The liquid wets the hydrophobic patterns due to these differences in the surface tension values. After the liquid settles on the surface, the system is suspended in the fluidic medium of different surface energy where the liquid-surface interface starts attracting the parts towards them as the result of capillary force ensuring proper alignment.

1.2.5.2 Binding Site Shape

The magnitude and directions of the capillary forces are determined by the shape of the binding site and the micro part as they have a significant role in the uniqueness of the assembly. The unique dependence of assembly in regards to orientation and accuracy

is explained by Xiong et al. in [13] based on first order approximation energy model. This explains the crucial dependence of capillary self assembly technique on the binding site design employed.

1.2.5.3 Liquid Volume

Liquid volume plays a significant role in accurate alignment of micro components by self assembly process. Unpredictable changes in the required volume have capabilities to affect the accuracy of alignment by either a tilt or a lateral displacement of the component. Thus appropriate control of volume of the liquid to be used is necessary for a precise alignment [7].

1.2.6 Modeling Capillary Forces in Self Assembly

K. A. Brakke came up with an interactive program called the Surface Evolver. The program is used for the analysis of surface shapes affected by surface tension, interfacial energy and other defined physical constraints. The evolution of the surface is by driving motion of the nodes on the surface to the minimum energy position. The software has the capability of defining surface tension, gravity, crystalline integrand, square mean curvature and other user defined integrals to represent the energies of the system. The program has capability to have a Riemannian metric so as to operate in space of arbitrary dimensions. It also has provisions to define spatial constraints and fixed constraints like fixed volume. The graphical output makes error identification easier and gives an idea on the iteration step involved.

Each vertex is defined and when the iterations take place they form small union of triangles for the evolution procedure. The vertices take in to consideration the degree of

freedom and the global scaling factor. The energy is calculated for each step. Numerous analyses are done on electrowetting and self assembly by using Surface Evolver [7, 14-16].

1.2.7 Electrowetting

Miniaturization increases surface to volume ratios bringing more challenges in control of surface and surface energies [17]. In microsystem engineering, microfluidics has tremendous opportunities with its capability to handle liquids in Micro optical switching devices, Micro RF switches, Micro fluid pumps, Digital Micro Total Analysis System (micro-TAS) and more [18]. A fundamental issue in microfluidics is the movement of fluid volumes as desired. Micro pumps offer one solution. However micro pumps require a variety of lithography steps for fabrication and helps in only a continuous flow. Another promising option is the phenomenon of electrowetting for the manipulation of individual drops.

In 1875, Gabriel Lippmann demonstrated a relationship between electrical and surface tension phenomenon. This relationship allows efficient control of shape and motion of a liquid meniscus by applying a voltage. The liquid changes shape when a voltage is applied in order to minimize the total energy of the system (sum of surface tension energy and electrical energy). Today, this effect, known as electrowetting, has seen potential importance in many applications.

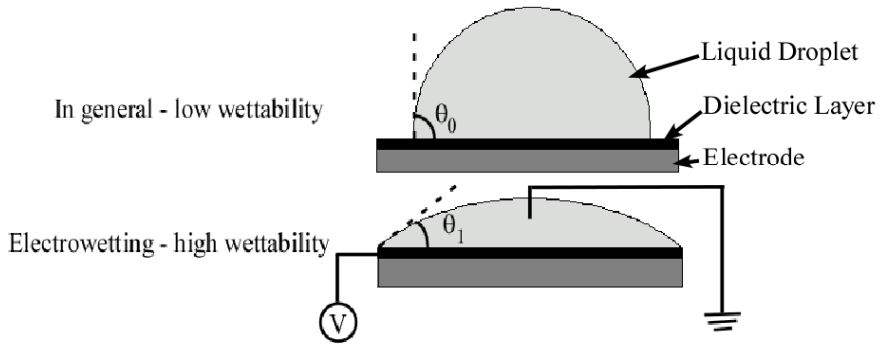

Figure 6 Representation of low wettability and their variation with applied voltage.

For efficient control of shape of the droplet, the surface energy of the surface over which the droplet is located should be controlled. The surface energy of this surface can be varied by varying the temperature, varying the chemical and topographical structure of the surface [19]. In miniaturized fluidic systems, electrowetting is an important source of electrical surface modification representing one of the best methods to control the liquid droplet.

The idea behind electrowetting is to make the surface highly wettable by an applied electric field. In electrowetting on a dielectric, the change of contact angle as a function of the applied voltage can be related to the dielectric thickness (δ) and dielectric strength ($\varepsilon_0, \varepsilon_R$) as proposed by the Young Lippman equation [17].

The system energy is found by modeling the fluid using the contact angle data and the Young-Lippman equation. The forces acting on the droplet are calculated by differentiating the energy with respect to the displacement of interest.

These predictions are computed with numerical modeling of surface forces using Surface Evolver [15, 16] in order to determine the sensitivity of the forces to variations.

$$\cos\theta_1 = \cos\theta_o + \frac{\varepsilon_o \varepsilon_r V^2}{2\gamma_{lv}\delta}$$

Equation 2 Young Lippman equation to show the dependence of contact angle with applied electric field.

Electrowetting is a unique method to realize the motion, dispensing, splitting and mixing of single droplets in a microfluidic system without the need of any mechanical or fault prone components. It employs control of voltage that changes the interfacial energy of the liquid-solid interface [17]. By alternatively applying voltage across an electrode, the fluid can be efficiently moved as desired, by changing contact angle of the liquid on the surface. This is proved by many works done so far by applying large voltage on dielectric called Electrowetting on Dielectric (EWOD) that provided large changes in the contact angle [20, 21].

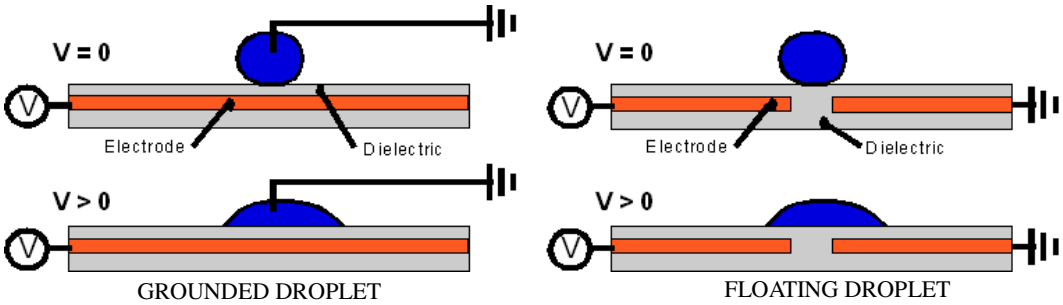

Figure 7 Most commonly employed configurations in Electrowetting.

Figure 7 shows two most common configurations employed in the electrowetting phenomenon. In the grounded droplet method, the liquid is grounded while in the floating droplet, the droplet floats across two electrodes with applied voltage across them. Both of these configurations produce an effective force on the liquid both in the lateral and

normal direction. This force induced is used to move the droplet through micro and nano tubes by alternatively applying voltage.

Crane et al. [22] demonstrated that a nanoindenter could be adapted to measure these fluid forces with a custom tip. This work is concerned with the sensitivity of such a measurement system to system factors including variation in liquid volume, angular alignment of the part and substrate and displacement of the part relative to substrate features.

1.3 Research Benefits

Self assembly is a promising alternative to conventional pick and place robotic assembly of micro components. Its benefits include parallel integration of parts with low equipment costs. Various approaches to self assembly have been demonstrated, yet demanding applications like assembly of micro-optical devices require increased positioning accuracy. This thesis implements a new method for design of self assembly bonds that addresses this need. Current methods have zero force at the desired assembly position and low stiffness. This allows small disturbance forces to create significant positioning errors. The proposed method uses a substrate assembly feature to provide a high accuracy alignment guide to the part. The capillary bond region of the part and substrate are then modified to create a non-zero positioning force to maintain the part in the desired assembly position. Capillary force models show that this force aligns the part to the substrate assembly feature and reduces sensitivity of part position to process variation. Thus, the new configuration can substantially improve positioning accuracy of capillary self assembly. This will result in a dramatic decrease in positioning errors in the micro parts.

Electrowetting is considered to be one of the most efficient methods to manipulate fluids through micro and nano tubes and in other high end applications. The forces induced in a system due to electrowetting can be measured through a nano-indenter thus making it an electrowetting force measurement system. This thesis will address the potential variations that can be caused in the force values obtained due to variations in liquid volumes, tilt of the part and lateral displacement. Influencing factors including voltage, methodology of voltage applied, changes in the liquid volume and effects due to the tilt in the component are considered in a detailed analysis. This analysis predicts the electrowetting behavior in different conditions under all factors that might affect the process so that guidelines for accurate measurements can be determined.

1.4 Thesis Outline

This thesis proceeds as follows. Chapter 2 reviews the previous works done in self assembly and electrowetting processes and summarizes their outcome. Chapter 3 details the analysis of capillary forces in a self assembly process and implementation of a new design approach of the fluidic self assembly bond for precision positioning of micro components. Chapter 4 is involved in analysis of capillary forces in electrowetting process and the sensitivity of the process to variations due to influencing parameters. Chapter 5 concludes the work done and recommends future aspects for improvement and optimization of the processes.

CHAPTER 2 LITERATURE REVIEW

2.1 Self Assembly

The concept of self assembly has been formulated since (1930). This is emphasized by many famous landmarks with those including the theory of universal Computation by Alan Turing (1930), The theory of automata replication by John Von Neumann (1950) and James D Watson and Francis Crick in the discovery of the structure of DNA [23].

While self assembly has been implemented in multidisciplinary fields since then, the potential of the concept came to lime light when Kazuo Hosokawa's group [23] demonstrated micro-scale self assembly using surface tension (1996). Since then there has been many research initiated in employing the concept of self assembly in the assembly of micro and nano parts.

Following those initial works, there were numerous efforts to validate, optimize and achieve a high precision assembly using self assembly process. This section details few of those important works under each category.

2.1.1 Optimization of Self Assembly Process

Zheng et al. [24] proposed the use of low temperature melting solder for assembly of functional LED micro components having three dimensional structures. The structure containted an LED component, an encapsulation body with solder bumps and a chip

carrier. The proposed technique contained an assembly sequence that shows the process involved in self assembly. This method combined the shape recognition and solder directed method of self assembly together to realize the necessity in multicomponent, multimaterial, three-dimensional microsystems. This method explored the option of assembling heterogeneous microsystems, three dimensional integration and ensured electrical connections. However the method was a sequential feed technique of feeding different sized components sequentially.

Cannon et al. [25] proposed the self assembly of millimeter scale parts into 5mm cubes of polymethylmethacrylate. This work describes about the local and the global energy minima in assembly and as to how the capillary forces acts as the driving force to ensure self alignment. The proposed method reports the self assemblies of parts with variety of functions being assembled in to three dimensional structures, enabled through a standard interconnect. An assembly rate of 0.125 components per second was recorded with a 93% yield. The problem of selective self assembly was reported. Process improvements such as using density stratified solution or molding alignment features so as to accept or reject parts by design were discussed.

Gracias et al. [26] demonstrated the phenomenon of self assembly to form interconnects in electronic devices especially in the circuits. The stages of series and parallel assembly in 3D electrical networks were established. By making the wires substantially narrower (approx 150μm) the height of the solder film was also limited. The width of the solder dots is 1mm. To ensure correct registration of parts, pattern to pattern registration was enabled by proper design of solder dots on the face of the part.

Xiong et al. [27] demonstrated a method of controlled multi-batch self assembly of micro components using capillary forces. An array of gold binding sites was patterned on the oxidized silicon substrate and once these sites are exposed to an alkanethiol solution, they become hydrophobic. The self assembly process was executed in an aqueous environment with a hydrophobic adhesive as the bonding fluid. Without a Self Assembled Monolayer (alkanethiol solution), the gold sites are inactive as the sites are hydrophilic. Hence the self assembly process is done by the principle of hydrophobic/hydrophilic interactions. The de-activation of Self assembled Monolayer is also discussed by application of an electrochemical potential between the gold and the aqueous solution. By this method the sites were able to be selectively assembled by selective activation and de-activation and thus obtained controlled multibatch assembly of parts. LED arrays were assembled on to the substrate with the heat polymerizable adhesive, and the electrical connections to the substrate were formed by electroplating tin and lead.

Fang et al. [14] proposed an assembly process based on shape recognition and capillary-driven mechanisms. The capability of this assembly towards various factors those including high dense assembly, peg free micro components, process in air environment, different modes of part mounting, unique face orientation of parts, assembly of different types of components with even similar dimensions and high surface coverage on the surface were considered and achieved using the proposed technique. For this proof of concept 790µm diced square silicon components were used. A parallel assembly strategy of the assembly sequence is detailed and the surface treatment of the diced parts to achieve the required assembly is also provided. Two different cases were

considered in terms of part dimensions (flat-edged parts and the step-edged parts) and the assembly strategy methods including vertical mode and the horizontal mode are considered. The process achieved 1000 densely packed parts in approximately 2 min and the defect rate is mentioned to be approximately 1%. A single batch proposed a surface coverage of 31% while the second batch doubled the same.

Another class of processes referred to as self assembly is the alignment of computer chips by the surface tension of solder during solder reflow. Vivek [28] proposed the analytical prediction of the shape and solder heights of equilibrium joints formed due to the solder re-flow in surface mount components. This is done for the application of the components to the printed circuit boards. For this analysis the two dimensional joints with negligible solder density effects are considered. Experimentations were done on the same and the results agree with each other. The sensitivity of the solder joint to the geometric and physical properties is analyzed numerically. Any smaller changes in these properties have larger potential heights at constant solder volume. The reliability of the solder joints is closely related to the characteristic properties. This proposed technique is highly helpful in prediction the shape of the solder and the stand-off heights when considering solder-based assembly.

Scott et al. [29] proposed a batch fabrication process to create a micron-sized helical and toroidal inductors with Q values greater than or equal to 50 at multi-GHz frequencies. In order to increase the value of Q the aspect ratio must be high as Q is directly proportional to the aspect ratio of the inductor. The self assembly process allows multiple interconnects to the inductor. A proper design of inductor was required so as to minimize the losses between the substrate and the conductor and increase Q and

operating range. The part and the substrate are selectively processed for hydrophobic/hydrophilic interactions. Such a design and assembly had led to an inductor with Q approximately 60 at 5 GHz and with a resonant frequency of 9 GHz. Such an inductor when assembled provides an increase by a factor of approximately three as compared to a traditional lithographically fabricated inductor.

Zheng W [30] proposed a novel assembly process to integrate and connect semiconductor dies on surfaces with Single-Angular Orientation and Contact-Pad Registration. In this proposed technique major concerns were to avoid overlaps in assembly, uniquely orient components and enabling assembly of parts of various dimensions. An experimental approach and results of the assembly process are detailed. A unique method of protecting five spots of gold surface with Shipley 1813 photoresist was necessary to ensure correct angular orientation. The fabrication procedure is detailed as part of the proposed technique and the assembly orientation and alignment issues are discussed by images of SEM and a standard deviation was measured for the lateral distance and the angular deviation for the proposed methods. The final results were an angular orientation of 0.3˚ and contact pad registration with an accuracy of 19µm for heterogeneous dimensions from (500µm – 2mm).

Most self assembly of micro components relies on the fluidic medium due to the fact that the handling of such small devices becomes highly difficult in air/dry environment. Yeh and Smith in 1994 [31], proposed a technique on fluidic self assembly based on shape matching between micro components and receptors with recess on them. The ability of the parts to recirculate across the receptor holes by constant agitation until they fall in to the receptors is the success of the fluidic self assembly. Integration of GaAs

surface-emitting laser components on silicon substrate was demonstrated using this technique. The substrate had etched holes in a trapezoidal shape with those similar to the parts. The GaAs along with the fluid medium is dispensed on the substrate. The required orientation is obtained due to the trapezoidal shape of the part and the site. Random mechanical vibration was performed to give the necessary agitation so as to position the parts in to the receptor sites. According to the proposed method more than 90% of the holes were filled with the GaAs blocks.

2.1.2 Achievements Towards Precision Self Assembly

Srinivasan et al. [5] demonstrated the self assembly of parts with submicrometer positioning accuracy. The lateral alignment and the rotational misalignment have been dealt with in the paper and the proposed method of fluidic self assembly. Different sized parts ranging from 150 x 150 x 15 μm^3 and 400 x 400 x 50 μm^3 were used in the assembly process and were directed towards the substrate using a pipette. The constraint of accuracy in the assembly process is attributed to the patterning of the hydrophobic shapes and thus the positioning depends on the resolution of these hydrophobic shapes. The substrate has been lubricated in the proposed method so as to eradicate binding of parts to each other as a result of capillary forces between them. A quartz substrate was used to assemble microparts so that the accuracy can be determined by picturing the parts through the transparent substrate. The proposed shape matching occurred in approximately 1 sec in the experimental verification of the proposed technique and the self assembly step is slowed by increasing the viscosity of the lubricant. The advantages of self assembly over wafer to wafer transfer were detailed and the maximum precision of 0.2μm and rotational misalignment of approximately 0.3° were reported with the

assembly rate of 98 part arrays in 1 minute with the yield of 100% is recorded by the proposed method.

Srinivasan et al. proposed a similar method of fluidic self assembly technique using capillary forces to assemble micro parts [32] with high alignment precision. For this purpose, a heat curable acrylate adhesive was used to provide capillary forces and is polymerized in a bath of water at 80˚C for 16 hours with continuous nitrogen bubbling. The fill factors were measured to be 95% and the assemblies were measured to be flat to within 6nm rms. Further improvement of the process are discussed with those including reducing the mass of the assembly parts, characterizing the adhesives and proper tune of bind site area to produce different levels of adhesion.

Singh B. P. et al. [33] proposed a technique to assemble laser diodes using a guided fluidic assembly with reduced problems of misorientation. Unassembled Laser diodes are guided through a 150 µm thick nickel metal mask in to the recess. Thus the assembly process is done in two steps. The first step is to guide the parts through the mask to the recess and the second step is the fine precision of the part under fluidic as well as gravitational force. Different sizes of Laser Diodes are assembled successfully with a precision of 2µm and 100% efficiency. A flow chart to detail the automation capabilities of the guided fluidic self assembly is provided. Once the parts are assembled, wafer heat treatment is done before performance characterization.

2.1.3 Surface Evolver in Self Assembly

Surface Evolver by K. A. Brakke is a powerful and flexible system to represent and solve for equilibrium surface profiles and energies. This program can be used to analyze liquid surfaces shaped by various energies including surface tension and can be

subject to defined physical constraint. Surface Evolver drives the defined surface towards minimum energy and calculates force induced within the surface as a derivative of the energy. Numerous works were done using Surface Evolver to predict the assembly liquid shape, to determine the characteristics of the process at different parameters and to analyze the process at different volumes. This section details a few of those works done using Surface Evolver which proves this program to be an efficient source for simulation and analysis of self assembly systems.

Andreas et al. [7] proposed a parallel assembly in the fluidic phase. The proposed technique was by controlling the hydrophobic and hydrophilic interactions between the part and the site. The considered geometry is a square shaped part and a similar binding site and the sites are coated with a hydrophobic alkanethiol layer. The principle of the assembly was by the difference in the surface energy of different medium in the assembly which acted as a driving force. A Surface Evolver model was simulated by giving the part a shift, a lift, a twist motion and a tilt. Results were generated and the assembly height corresponding to a volume of 200 nl is 0.174mm. The critical importance of the lubricant volume was portrayed in this work and a tilt deformation in the part was shown with increased volume. The concept of increase of restoring force with various shifts and then attaining a saturation value was proved. The Surface Evolver model was proved to be effective in predicting the final assembly shape and location to characterize the self assembly process.

Harsh et al. [34] explored the use of liquid solder to move a MEMS mirror from its planar fabrication position to an out-of-plane operational position. They developed a Surface Evolver model to predict the final assembly equilibrium angle of the solder,

which was proved to be within an error of +/- 2 degrees based on experiments. The modeling of the same obtained better results on these error values giving high potential of Surface Evolver to aid in designing innovative 3D MEMS devices assembled using solder. This process of assembly of MEMS devices uses surface tension of solder. As stated earlier in [7], there is a crucial dependence of solder volume in the assembling accuracy. Hence the proposed technique explains the importance to develop and design models for solder at demanding precision requirements. A comparison of geometry based model and a surface energy-based model are also presented. Various model aspects were considered and corresponding details are predicted for geometry based model and Surface energy based model. The need for a static analysis to consider potential energy was stated. The paper demonstrated the proposed technique with 15 test assemblies.

Sean et al. [12] proposed a two stop process with a finite element model to predict the hydrodynamic forces that would move the part towards the substrate and the Surface Evolver program to determine the efficient assembly of the part once it comes into contact with the binding site. For the proposed model the binding site is designed with 10µm and 20µm deep recess and contains a low melting point solder on metal pads at the bottom of wells. Silicon shapes carrying matching patterns were used for assembly testing procedure. A simulation is performed in the FEMLAB model to identify if the viscous fluid forces would be sufficient to move the component to the desired location. Once the component reached the desired location, modeling is done to predict the alignment of the component in the well. The results showed that the fluid forces induced were very small (between 2.5 and 2nN) for the component dimensions of 10µm x 50 µm x 300µm. The results also predict a decrease in the fluidic force once the liquid reaches

the desired location. The Surface Evolver model gives a prediction of the force at various lateral distance and heights once it is in the site. The simulation results were confirmed with those of the experiments.

2.2 Electrowetting - Review

Recent emphasis on microscale phenomena and devices has resulted in many microscale fluidic systems. Most of the devices and methodologies developed focus on continuous motion of fluid medium on a solid surface through a closed channel. However, recent advancements have paved the way to individually manipulate liquid droplets [17, 35, 36] in a process termed *digital microfluidics* (DMD). Electrowetting is the primary tool for manipulation of individual microscale liquid droplets. In this section, we review recent works that focuses on droplet motion and control and the force induced in the method.

Lienmann et al. proposed [15], a simulation using Surface Evolver to study the detailed behavior of a droplet for a given electrode geometry and voltage curve. The proposed work mainly dealt with the simulation to predict the electrowetting effects on a droplet and a methodology to calculate the shape of electrodes and optimization of the same was predicted. The results were compared with those of the analytical model. The simulations are integrated to a user-friendly simulation tool based on Surface Evolver code. The application was focused towards four operations including creation, motion, splitting, mixing/merging of droplets. The proposed work helped in understanding the electrowetting behavior and proved the reliability of the process.

Baird et al. proposed [37], a method to examine electrostatic force on microdroplets transported via Electrowetting on Dielectric (EWOD). The force

distributions on advanced and receding fluid faces are detailed in each case. Dependence of the force distribution and its integral on system geometry, droplet location and material properties are described. A comparison of scaling properties and force distribution for both the cases are given. The effect of the divergent charge density on possible explanations for contact angle saturation such as charge trapping, local dielectric breakdown, and corona discharge are also studied. Both analytic results for integrated total forces and numeric results for the force distribution are compared and are proved to be in agreement with results over the other.

Walker et al. [38] discussed the modeling and simulation of a parallel electrowetting on dielectric device that studies droplet movements through surface defects. The simulations are compared to that of the experiments for a splitting droplet. Various factors affecting electrowetting effects are considered and the details on their influence are described in detail. The governing fluid equations and boundary conditions along with contact hysteresis are developed. A numerical simulation is described which uses a level set method for tracking the droplet boundary.

Peykov et al. [39] developed a model to study the contact angle changes and the limit at which the contact angle saturation occurs. The model proposed in this work predicts that for an electrowetting device in which an aqueous droplet can be forced to completely wet a hydrophobic surface, a surface with the same surface energy as the liquid is required. Indeed the work presented a more detailed consideration of electrowetting taking in to account the detailed structure of the double layer.

Berthier et al. proposed [40] a technique to find to investigate minimum and maximum actuation voltages in electrowetting. He formulated maximum voltage as a

threshold beyond which there is no more gain in the capillary effect due to the saturation effect. Calculation was done to determine the electrowetting force on a EWOD system considering the contact angle hysteresis and an analytical relation was obtained to derive the minimum actuation potential.

CHAPTER 3 DESIGN OF FLUIDIC SELF ASSEMBLY BONDS FOR PRECISE COMPONENT POSITIONING

3.1 Introduction

Assembly is essential to the production of most manmade products. The challenges of design, engineering, manufacturing and logistics come together as individual components are combined to make a functioning system. In macro-scale applications, assembly processes have relied on human and robotic assembly to place, interconnect and integrate components at all complexities. Robots are efficient for the accuracy and repeatability that were achieved and hence high precision assembly was possible at the macro-scale.

With the evolution of micro-manufacturing in recent years, part size has been greatly reduced. Although Robotic assembly is highly efficient at the macro-scale, it loses its efficiency at the micro-scale due to increased positioning control challenges and difficulties in grasping and releasing micro-scale components. This is due to the fact that the surface tension, Van der Waals, and electrostatic forces dominate the gravitational force at the micro-scale. Moreover such a serial assembly by robots may not be time efficient and there are more complications while considering 3D integration of components especially at the micron level. This creates a tremendous demand for new micro-assembly techniques in both packaging and integration of complex microsystems.

Recent developments in micro assembly technologies include micromanipulator based assembly [1], pick and place method [41] and wafer to wafer devices transfer [2]. The limitations of these methods included challenges of precision assembly, poor performance on non-planar surfaces in cavities and in fabrication of 3D systems and lack of a parallel assembly approach. While wafer to wafer transfer achieves parallel integration, yields can be decreased due to integration of potentially defective components with functional components.

Self assembly is a promising alternative technique to conventional micro assembly methods. It is a parallel assembly approach with 3D integration compatibility and it requires limited specialized equipment. This can be applied to known good parts and unused or misassembled parts could be recovered and recycled to improve the assembly yields. In self assembly, components are brought together through random interactions. Over time, the system minimizes its energy by bonding together in the desired configuration. Self Assembly processes are often classified by the dominant interactions. These include electrostatic [8], magnetic field [9], and surface tension driven self assembly [13, 26, 42].

Surface tension-driven self assembly is achieved by the reduction of surface energy of an assembly fluid. Common assembly fluids include water, adhesive, and solder [7, 14, 29]. The surfaces of the parts to be assembled are patterned to create regions with differential wetting characteristics. An assembly fluid is introduced onto the well-wetted surfaces. These are dispersed in an immiscible fluid and agitated. The system energy is minimized when the assembly fluid contacts other well-wetted surfaces and the parts are bonded together. The physical location of the minimum energy

configuration depends on parameters such as the surface tension, shape of the wetting regions, and the volume of the assembly fluid. In general, these must all be managed to assure accurate part positioning [7].

The promise of self assembly has motivated a variety of trials. These have shown that it is possible to assemble significant numbers of parts successfully in short periods of time. Fang et al. [14] demonstrated assembly of 1000 densely packed receptor sites with micro parts in about 2 minutes with a defect rate of approximately 1%. Many studies have not measured the positioning accuracy of the components, but Srinivasan et al. [5] demonstrated assembly with a precision of less than 0.2μm and a rotational misalignment less than 0.3˚. Singh et al. [33] assembled laser diodes of two different sizes with ±2μm precision. Zheng et al. [30] proposed a novel technique to assemble different sized components with 0.3˚ rotational precision and a potential method to avoid some common assembly errors. The eventual range of self assembly applications will depend on the accuracy with which parts can be assembled and the process control that is required to achieve these levels. Demanding applications requiring precise optical alignment or electrical connections with a small pitch require further improvements in positioning accuracy. This work presents a concept for improving the accuracy and repeatability of positioning through self assembly and analyzes one method of implementation. A particular advantage of this method is its ability to reduce sensitivity of part accuracy to many sources of process variation.

3.2 Basic Concept

All systems evolve towards their minimum energy configuration. S*elf assembled* systems are designed so that, the perfect alignment position is coincident with the global

energy minimum. The system evolution toward this position is driven by an effective force that is equal to the derivative of the system energy with respect to displacement. The net force at the alignment/equilibrium position is zero since the energy is at a minimum. Although this phenomenon of energy minimization drives assembly, accuracy is limited by the change in the energy landscape due to process variation. These include variations in surface energies, dimensions, liquid volumes, and disturbance forces such as gravity, inertia, and electrostatics that can affect both the minimum energy position and the part sensitivity to variation.

Figure 8(a, b) illustrates a basic prismatic part assembled to a substrate via surface tension driven self assembly. The impact of process variations can be seen by analyzing the surface tension bond as a combination of springs connecting rigid parts (Figure 8(c)). The position is a function of the disturbance forces and the spring stiffness—both of which can vary. Together, these can create significant errors and uncertainty in the part position. Figure 9(a) illustrates the errors that result from a disturbance force and the uncertainty in the error motion due to variation in the spring stiffness. Accuracy improvement requires that all of these variations be minimized or that the system sensitivity to the variations be reduced. Even weak forces or torques can introduce positioning error by changing the position of the energy minimum.

Macro-assembly systems utilize stiff alignment features to assure accurate positioning despite variations in some parameters. Springs or other compliant parts are then used to hold the part against the alignment guide. This can be implemented in the spring model of Figure 8(c) by introducing a physical constraint that displaces the part from its equilibrium position as illustrated in Figure 8(d). A restoring force of magnitude

$k\delta y$ is obtained. This force pushes the part towards the energy minimum while the high stiffness of the rigid constraint prevents movement. Due to the large difference in stiffness between the alignment guide and the spring, the alignment guide is considered a rigid body. Disruptive forces below this restoring force, referred to as the preload *force*, will not displace the part. The magnitude of the preload force will be a function the effective spring constant and the global equilibrium position, but the part position is independent of these variations over a significant range. The resulting force-displacement error relationships are similar to the schematic shown in Figure 9(b).

Thus, the accuracy of the part position is a function of the accuracy and repeatability of the alignment feature alone. The spring's sole function is to hold the part against the positioning constraint. Variations in spring stiffness and the zero force position of the spring over a significant range now have no impact on the part position. The system should be designed so that the preload force is greater than any expected disturbance forces and the accuracy of the alignment feature should be within the required positioning accuracy. Under these conditions, the part position can be considered independent of these system variations as in Figure 9(b). This is the concept of "force closure" articulated by Whitney [43].

This insensitivity to variation would be of particular value in self-assembled systems at the micro-scale. Many sources of process variations are difficult to control. For example, surface energy affects both the effective spring stiffness and equilibrium position and can be very sensitive to surface contamination. Also many current methods of applying the assembly fluid require tradeoffs in control of the fluid volume versus

speed of application. Further, self assembly processes rely on random interactions to generate the assembly which can also be a source of process variation.

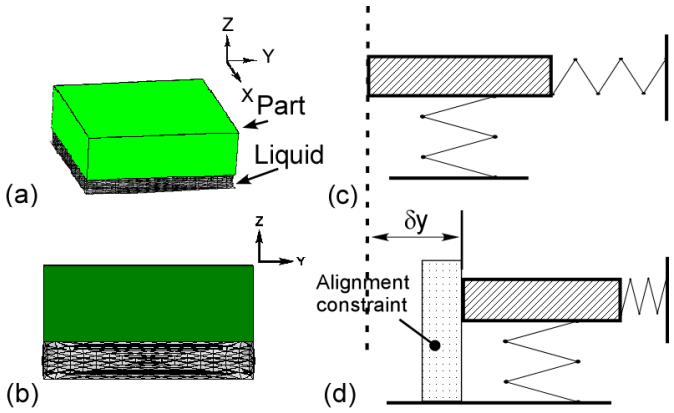

Figure 8 (a) Typical self assembly system (b) proposed self assembly system (c) mass-spring system representing typical self assembly system. All disturbance forces deflect the springs and move the part. (d) mass-spring system representing proposed self assembly system. An alignment constraint displaces the part to create a preload force. Only disturbance forces above this preload can displace the part.

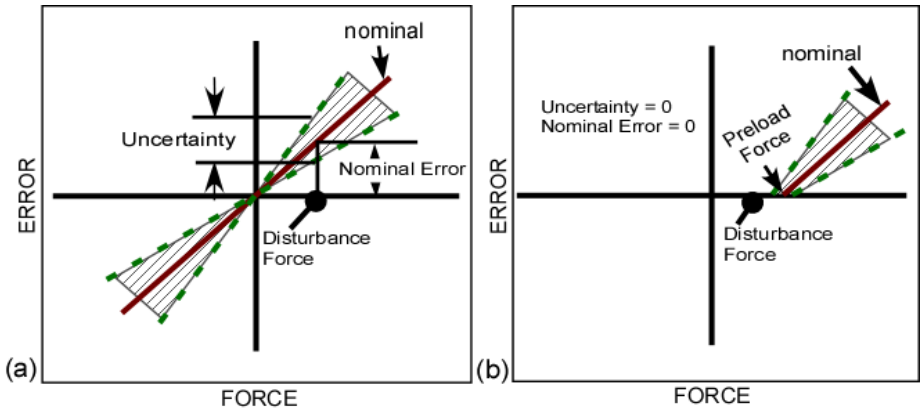

Figure 9 Representation of error corresponding to force disturbances in self-assembled components. (a) Typical self assembly bond. In the typical self-assembled cases, all disturbances create variation in the part location. (b) Force-closure part positioning. The introduction of a rigid alignment feature decreases the error and uncertainty in position for disturbance forces below the preload force.

This force-closure concept can be implemented in self assembly systems to reduce the sensitivity of micro self-assembled part positioning to process variation. In a capillary self assembly system, this can be accomplished by introducing a rigid alignment feature to constrain the part. The wetting pads of the assembly fluid are then designed to

reach their minimum energy position at a point that is blocked by the alignment feature just as the feature in Figure 8(d) prevents the spring from reaching its undeflected position. The fluid will apply a continual preload force against the alignment feature. In this work, the preload force is created by introducing a difference in dimensions of the substrate with respect to the part. The magnitude of this dimensional difference is referred to as the *dimensional offset*.

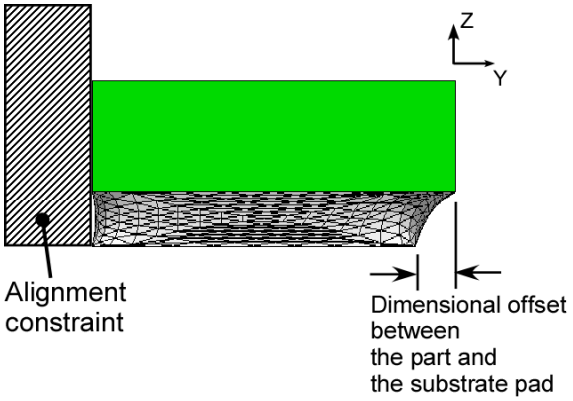

Figure 10 Proposed self assembly system to establish force-closure concept in micro-scale. The wetted region on the part is larger than the wetted region on the substrate. Without the alignment constraint, these part would move to the left so that the center of the two regions were aligned. However, the alignment constraint prevents this motion and thus creates a preload force against the constraint.

The alignment feature can be any rigid feature that provides the appropriate constraint. In the 2-D case, this can be a simple block as shown in Figure 10. One or more alignment features can also be used to provide constraint in multiple degrees of freedom. If the fluid bonds are appropriately designed, a preload force can be created that maintains the part position against the constraint in all the required degrees of freedom. For the planar case, this can be accomplished by creating a dimensional offset in both the x and y axes. The forces and equilibrium positions have been analyzed for dimensional offsets in both one and two dimensions. The results are presented below.

3.3 Simulation

The simulation of a basic self assembly bond is done in Surface Evolver; a powerful and flexible system for representing and solving for equilibrium surface profiles and energies. The program analyzes the liquid surfaces shaped by various energies including surface tension subject to defined physical constraints. The program drives the defined surface towards minimum energy by the gradient descent method. Numerous works have been done using Surface Evolver to predict critical parameters of the self assembly process including positions and forces [4, 7, 13].

Due to the small sizes of the components and the relative strength of the capillary forces, the inclusion of gravity in the simulation has negligible impact on the analysis under the conditions studied in this work except where noted below. Therefore gravity is neglected in the analysis unless otherwise indicated. The interfacial energy values defined in the system for Liquid-vapor (γ_{LV}), Solid-vapor (γ_{SV}) and Liquid-solid (γ_{LS}) are 46e-3 J/m^2, 52e-3 J/m^2 and 1e-3 J/m^2 respectively to represent an interfacial energy system analyzed by [7]. Dynamic effects such as kinetic energy and viscous losses are not considered in the simulation.

The model defines a fixed wetting region that represents the assembly substrate. The part is represented by a square pad with six degrees of freedom (three translational and three rotational motions). A liquid surface is defined between these two. Boundary constraints are defined to constrain the liquid within the contact regions and the appropriate surface energies are applied to each surface. The Surface Evolver is used to find the equilibrium shape and energies of the liquid surface. Forces and torques are found from the Surface Evolver energy calculations by taking the derivative of energy

with respect to the position variables of interest using the central difference method. An optimization routine within the Surface Evolver model finds the equilibrium position of the part relative to the substrate. This is done by iterating on the z-displacement and rotational degrees of freedom of the part to minimize the surface energy of the system for a specified position in x and y. The desired assembly position is defined as the origin of the coordinate system. Force-displacement relationships are obtained by applying displacement offsets and solving for the forces at each position. The Surface Evolver models do not directly include the effects of alignment features. These are modeled by assuming that the part motion is limited at some displacement level. In this work, the alignment features are positioned to prevent negative x and y displacements. However, force results are calculated for these negative positions to illustrate the overall fluid response.

The parts analyzed in this study are 900 μm x 900 μm. The assembly fluid is assumed to wet the entire bottom face of the part while the substrate has a rectangular wetted region that is varied in size to create different dimensional offsets. The fluid volumes used in this study created fluid heights from approximately 100 to 250 μm. When comparing designs with different dimensional offsets, the volume was scaled with the size of the substrate pad. These models were used to study the impact of varying position, fluid volume, and dimensional offsets between the pad and substrate to characterize the proposed fluidic assembly system. The impact of dimensional offsets on restoring forces and tilt errors are analyzed to identify their relative sensitivity to disturbance forces and volume variation.

3.4 Results and Discussion

The Surface Evolver models were used to predict the force-displacement relationships of self-assembled parts with different values of dimensional offset in the y-direction. Figure 11 shows that the forces in the x and z directions are zero to within the limits of the Surface Evolver convergence while the y-force varies both with displacement and dimensional offset. In the typical self assembly configuration, dimensional offset=0, Figure 11(a) shows that the y-force is zero at the desired assembly location ($\delta y=0$). A 100 micron dimensional offset creates a restoring force of approximately 27.6 μN at the assembly position

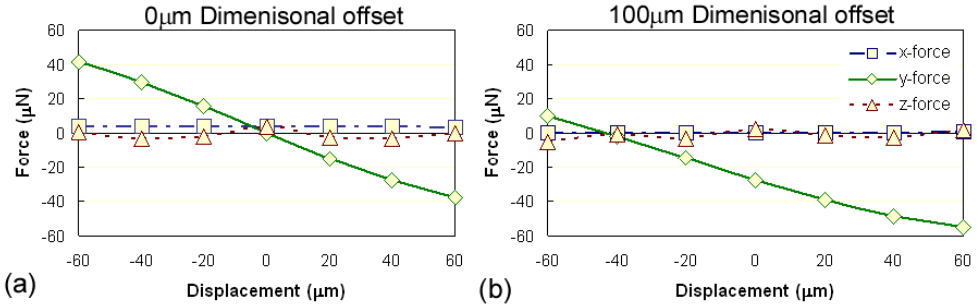

Figure 11 Surface Evolver predictions of force versus y-displacement for different values of dimensional offset. (a) Dimensional Offset = 0. At the desired assembly position, there is no reaction force. (b) Dimensional Offset = 100 μm. At the desired position, the liquid applies a force of approximately 27.6 μN. Forces below this critical force will not introduce any positioning error.

This would be the preload force for the selected parameters. Disturbance forces below the preload force will not cause any motion in the parts. The force reaches zero at approximately -40 μm displacement. This point would be the energy minimum location, but this position is not attainable in practice due to the alignment features. Thus, the zero displacement position is the actual minimum energy location achievable in practice.

3.4.1 Force Variations with Displacements for Different Dimensional Offsets

As seen in Figure 12, the preload force continues to increase with increasing values of the dimensional offset until it reaches approximately 37μN. The variation in tangential force with displacement can be estimated from simplified representations of the capillary force. The liquid will exert a force on the part equal to the surface energy times the perimeter length. The force will be oriented tangent to the liquid surface. The y-force is then given by the perpendicular edges of the rectangular part. If the surface is modeled as a plane, there is no horizontal force contribution from the left side of the fluid because its tangent is vertical. The out-of-plane (z) component of the force is balanced by the internal pressure in the fluid. The maximum force is obtained when the fluid is tangent to the part and the angle θ goes to zero and is approximately 41μN for this case.

The planar force can be estimated as a function of the dimensional offset as

$$F_{py} = L\gamma\cos\left[\tan^{-1}\left(\frac{h}{\delta V}\right)\right]$$

Equation 3 Prediction of preload force for one-dimensional offset.

Where

F_{Py}	-	Preload Force in the y-direction (μN)
L	-	Width of the part (μm)
γ	-	Surface tension (J/m^2)
h	-	Height of the liquid (μm)
δV	-	Dimensional offset in y-axis (μm)

Figure 12(b) shows that these relationships provide adequate estimates of the limits and trends of the preload force. Preload force increases with increase in the dimensional offset up to approximately 200 μm dimensional offset. Beyond this offset no further increase in preload force is observed. However, the accuracy is limited because

the actual fluid is not well-approximated by a plane. For analyzing the model for the effects of forces and tilt, a dimensional offset of 100μm is considered.

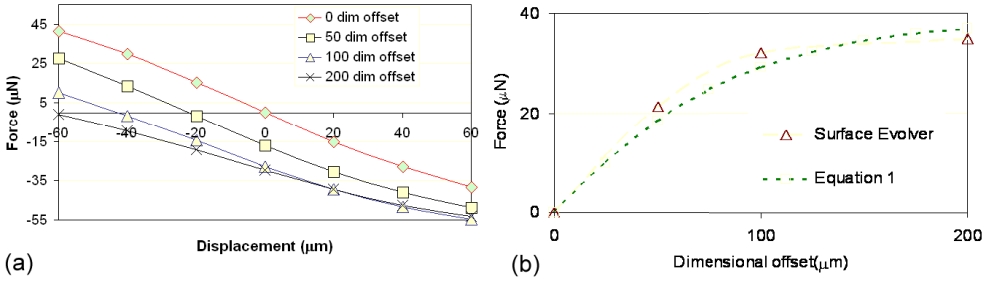

Figure 12 Impact of dimensional offset on part forces. (a) Variations in the force-displacement relationship for four different values of dimensional offsets. Larger dimensional offsets increase the preload force but with diminishing benefits above 100 μm (b) Variation in the preload force with dimensional offsets. Equation 1 provides an adequate estimate of the preload force over the range of dimensional offsets analyzed.

3.4.2 Potential Error Sources

The introduction of a dimensional offset disrupts the symmetry of the self assembly bond and could introduce additional angular errors into the part position. This was evaluated by calculating the equilibrium angular orientations using Surface Evolver. According to the analysis, the tilt errors in the part ranged to a maximum of 1 ± 0.2 ° in a typical self-assembled system. Greiner et al. [7] showed that in capillary self assembly, the flat position is an unstable equilibrium. Thus, the parts tend to tilt about one axis to reach a stable energy minimum. When a 100 μm dimensional offset is introduced, these tilt errors are unchanged.

This estimate of angular error was obtained while only considering the impact of alignment position on the location of the part center. An actual alignment feature like the one illustrated in Figure 10 would constrain both the y-position and the rotation about the z-axis. Thus, it is expected that rotational errors in the x-y plane will be very small. If

large x-axis or y-axis rotational errors were observed for parts under some circumstances such as parts with large mass, these could be reduced by the introduction of additional alignment features to constrain these axes. Gravitational forces do not significantly change the rotational errors at the desired assembly position, but do have larger effects with increased part displacements, larger dimensional offsets, and or larger assembly fluid volumes. Under these circumstances, gravitational effects should be considered.

Previous research has shown that the part positioning can be sensitive to the assembly fluid volume [7]. For both the typical assembly configuration and the force-closure configuration, the part height varies linearly with fluid volume over most volumes of interest. The preload force also varies significantly with the volume of the assembly fluid. For the 100 μm dimensional offset, the preload force decreases from 32.0 μN to 19 μN when the volume doubles from 63 nl to 126 nl. However, if the nominal preload is maintained greater than the expected disturbance forces, the part position can still be insensitive to the fluid volume variations.

3.4.3 Dimensional Offset in Two Axes

The results presented above explain the characteristics due to dimensional offset in one dimension (y-axis) of the part. This concept can be extended to include dimensional offsets along both x and y axis of the part to produce a resultant force in both directions. This preload force acts along the resultant direction of the defined dimensional offsets. By implementing dimensional offsets in both the dimensions, disturbances forces in both axes can be overcome and stability can be improved further. Figure 13 illustrates how this could be implemented. The force-displacement relationships vary depending on the direction of motion. Figure 14 shows how the forces compare for motion along the

y-axis alone and for equal displacements in the x and y-axis. The two-offsets respond similarly to the one dimensional case and they act nearly independent of each other. When displaced along the y-axis (Figure 14(a)), the x-axis force remains constant while the y-axis has a similar trend to the one-dimensional offset case. When the part is displaced at 45 degrees, both the x- and y-forces are of equal magnitude as shown in figure 7(b).

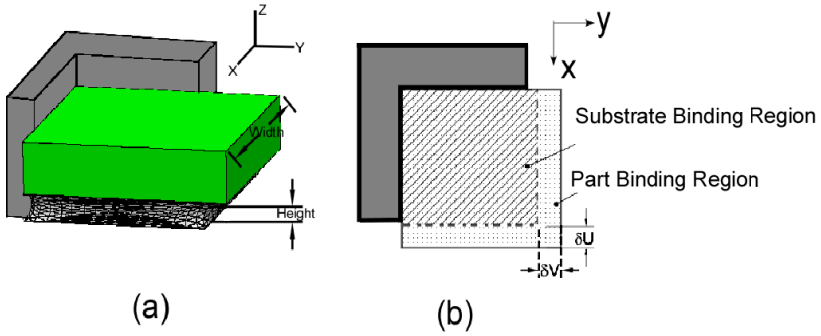

Figure 13 Representation of dimensional offsets in two dimensions. By creating dimensional offsets in two directions, preloads are created against the alignment constraints in both directions.

However, there is a significant difference in the change of the preload force with increased dimensional offset. Now, larger dimensional offsets decrease the contact angle of the fluid on the part, but they also decrease the length of the wetted region. Equation (1) is modified to obtain a revised preload force relationship of

$$F_{Py} = (L - \delta U)\gamma \cos\left[\tan^{-1}\left(\frac{h}{\delta V}\right)\right]$$

Equation 4 Prediction of preload force for two-dimensional offset.

Where δU is the dimensional offset in the x-axis (μm). A similar equation can also be written for the preload in the x-direction. Now the preload force is maximized at an intermediate value of the dimensional offset. At larger dimensional offsets, the benefit of a reduced angle of the fluid is offset by the smaller wetted length. Figure 15 shows

that this simple model provides an adequate representation of the variation in the preload force with dimensional offset for most design calculations.

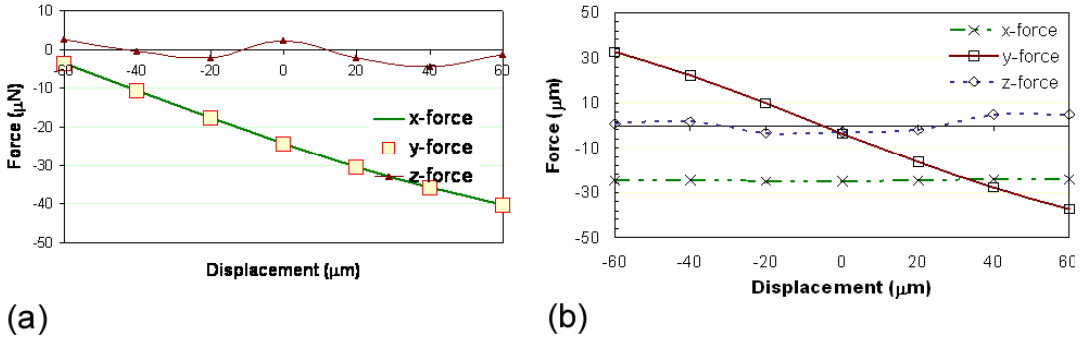

Figure 14 (a) Force in (x, y and z directions) versus displacement with 100μm dimensional offset in both x and y axis. The forces are the same in both directions. (b) Force in (x, y & z directions) versus y-displacement with 100μm dimensional offset in x- and y-axes. The x-force is constant as the part is displaced in the y-direction.

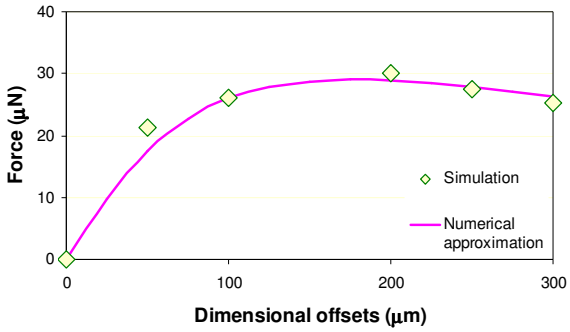

Figure 15 Variation in the preload force with dimensional offsets. The preload force reached a peak and then decreases with increased dimensional offset. Equation 4 provides an adequate prediction of the preload force.

CHAPTER 4 FORCE ANALYSIS ON ELECTROWETTING

Electrowetting is an effective method to manipulate droplets in Digital Microfluidics. The forces induced due to the principle of electrowetting is the main source of control of these droplets by causing an apparent change in the surface energy due to the voltage applied across the substrate on which the droplet is located. These forces induced can greatly affect the performance of electrowetting devices. Therefore, force measurement and optimization are critical to process improvements. A novel method has been developed to measure these forces in two-dimensions. This chapter analyzes the sensitivity of this force measurement method to variations in those parameters that affect actual measurements. The results obtained gives great insight to guide the design towards an improved measurement method and to estimate the measurement errors that could be caused due to the variations discussed.

4.1 Electrowetting Forces

In the case considered here, the droplet is positioned over two substrate electrodes with an applied voltage across the electrodes that can be varied. This creates a circuit with two capacitors in series. At steady state, the resistance of the fluid can be neglected so that the electrical circuit consists of just the capacitors. This setup was used in the force measurements from nano-indentor by Crane et al. in [22]. With a constant voltage across the electrodes, the voltage between each electrode and the droplet will depend on

the capacitance of the two capacitors. The capacitance is a function of the area of overlap of the drop and electrode which changes with position. Two different voltages are obtained on the left and right of the electrode. If the dielectric layer has a constant thickness and dielectric constant, the voltage induced on the left and right electrode can be calculated from

$$V_{LEFT} = \frac{A_{RIGHT}}{A_{LEFT} + A_{RIGHT}} V_{TOTAL} \qquad V_{RIGHT} = \frac{A_{LEFT}}{A_{LEFT} + A_{RIGHT}} V_{TOTAL}$$

Equation 5 Prediction of induced voltage on either side of the electrodes.

Where V_{TOTAL} is the total voltage applied to the system, A_{LEFT} and A_{RIGHT} are area of the electrode under the droplet on left and right electrodes respectively. The area influenced by the applied voltage depends on the position of the droplet. Hence voltage on each side of the electrode is a function of area which in turn depends on droplet position. Another behavior that can be observed during electrowetting is by the presence of a hole in the dielectric layer. A hole would short the capacitor on one side so that no voltage will be applied across the region of the droplet over the shorted electrode. There will be full voltage drop across the other side. In this case, the electrowetting force will be constant with displacement. The geometry considered for the analysis of the basic configuration of electrowetting force measurement is similar to [22] as shown in Figure 16.

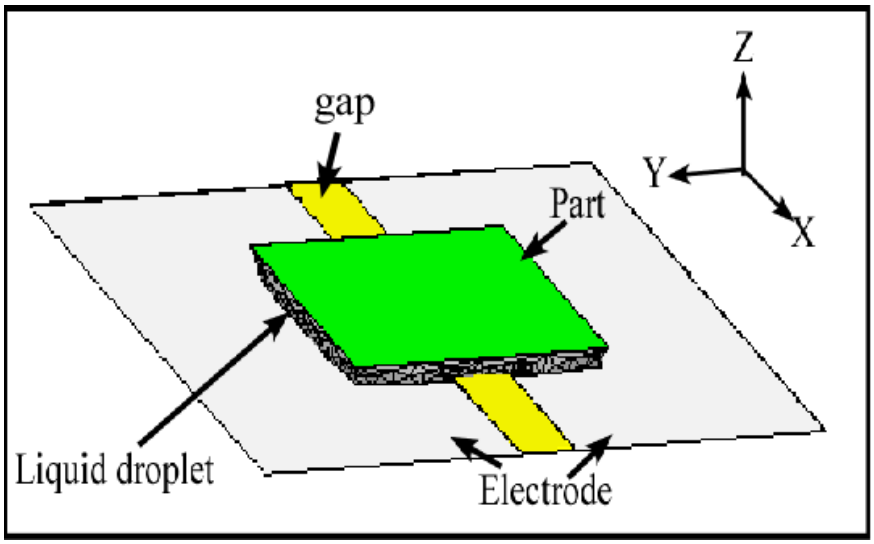

Figure 16 Surface Evolver model for force analysis on electrowetting.

In the previous work, Electrowetting forces were measured using a custom tip in a Hysitron Triboindenter in [22]. The top plate in Figure 16 was fixed to a nanoindenter. A small liquid drop is introduced between the plate and the substrate. The liquid and substrate materials are chosen so that the liquid completely wets the top plate. When the space between the plate and the substrate is small, the liquid is constrained by the shape of the top plate.

When a voltage is applied, the equilibrium position of the plate changes. Since the plate is restrained by the tip holder, the fluid applies a force on the plate in the direction of the minimum energy configuration. Due to the symmetry of this arrangement, the forces should be predominately in the 'Y' and 'Z' directions. The magnitude of these forces as predicted by numerical models can be closely approximated with simple formulas for the ideal case as demonstrated [22]. However, errors in alignment or changes in droplet volume by evaporation can cause variation in these electrowetting forces and depart from the ideal case. This Chapter will consider the impact of these variations on the force measurements. Electrowetting forces in both the

normal (two capacitors in series) case and one with the short (a single capacitor) are analyzed. The required standards and accuracy at which measurement needs to be taken in order to achieve precise measurements are detailed with the results obtained to support the explanation.

4.2 Electrowetting Force Analysis

Although the experimental setup measured the electrowetting forces, the alignment accuracy of the top plate to the substrate is unknown. There are always force variations that might cause variations/deviations from actual measurements. Also methods employed for control of liquid volumes were not very efficient and hence the force predictions due to minimal changes in volumes have to be considered. The test configuration was modeled using Surface Evolver and a detailed analysis is reported based on the predicted results.

The model used for simulation has a part and the substrate with the liquid in between them as shown in Figure 16 above. There is a gap between the electrodes. The gap between these two capacitors is typically 2mm and the height defined between the part and substrate is 580μm. The volume of the liquid used in the simulation is 47μl. The size of the part considered is 9x9mm in dimension and assumed to be a rigid body for ease of modeling. The substrate is defined based on the parameters of electrowetting and the part above the liquid is defined in a local frame of reference with six degree of freedom (three translational and three rotational). The translational motion of the part defined in our analysis is termed as offset and the rotation as tilt throughout the section. Both these motions can be defined to some constant value and force induced on the part due to electrowetting can be analyzed from the energy gradients as before. At the initial

position (0mm y-offset), the part center is positioned over the center of the gap between the electrodes. The voltage on each side is calculated using Equation 5 where the areas are calculated numerically in Surface Evolver. Typically in the floating case the voltage induced due to the applied voltage should be equal on both the sides as area under the droplet on the substrate is equal on both sides.

4.3 Results and Discussion

To begin with, simulation is run to analyze force in the y-axis against different values of voltage at 0 mm y-offset. With such a setup, in the normal configuration, the y-force is zero as the voltage is increased. But if there was a hole in the dielectric layer, the response is changed. A zero offset can induce y-force even at the 0mm y-offset as shown in Figure 17(a). This distinct difference permits easy detection of defects in the dielectric layer. Similar analysis is done at 3mm y-offset and the configuration with short on one side generates greater force than that of the normal configuration.

The y-force varies linearly with y-offset in the normal configuration as seen in Figure 18. This is because the voltage generated is dependent on the area of the droplet under the electrode. While a normal configuration gives a linear force variation with displacement, the force of that in a shorted setup is a constant with offset. This is due to the fact that the voltage is not applied to one of the side of the electrode and hence force induced is not linear with offset.

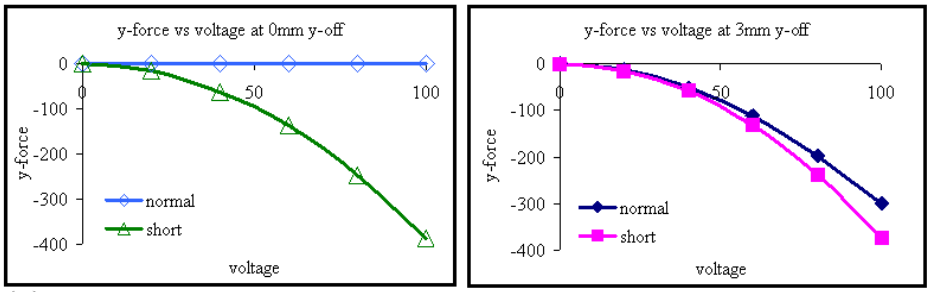

(a) (b)

Figure 17 Surface Evolver predictions for comparing normal configuration and the configuration with hole on the dielectric layer on one of the sides. (a) comparison of y-force vs. voltage at 0mm y-offset. (b) Comparison of y-force vs. voltage at 3mm y-offset.

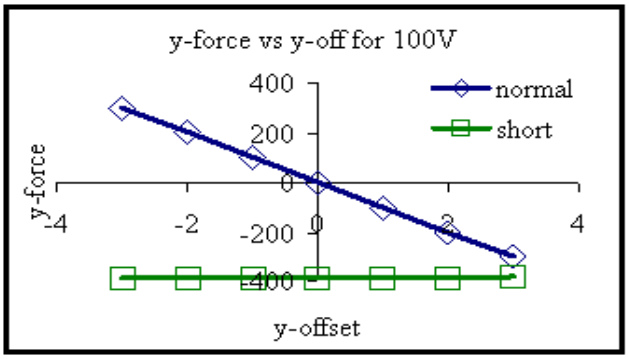

Figure 18 Comparison of y-force vs. y-offset at 100V for normal configuration and one with short.

4.3.1 Effect of Tilt

When force measurements are done in the electrowetting setup, the alignment of the top plate with respect to x, y and z axis are assumed to be parallel to the substrate. In reality this may not be true and hence there might be variations in the measured value of force due to misalignment of the top plate with respect to the substrate. The sensitivity of the force measurements due to misalignment in the plate is detailed in this section with results to support the analysis. Tilt about the three axes will be considered separately. Figure 19 illustrates tilt about each axis using output from a Surface Evolver model.

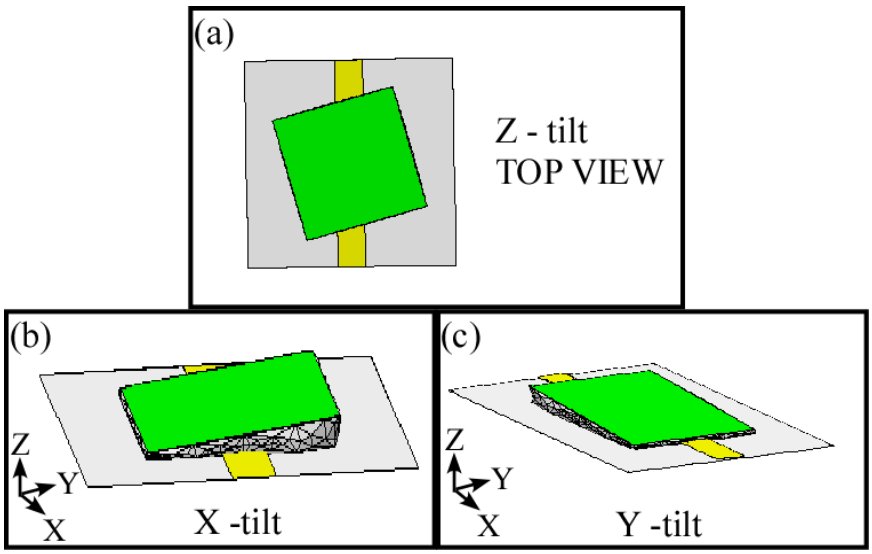

Figure 19 Surface Evolver model to detail tilt in different axis (a) z-axis (b) x-axis (c) y-axis.

4.3.1.1 Z - Tilt

Tilt in the x and y-axis are defined to be zero while the *z-tilt* is increased in steps to measure force variation.

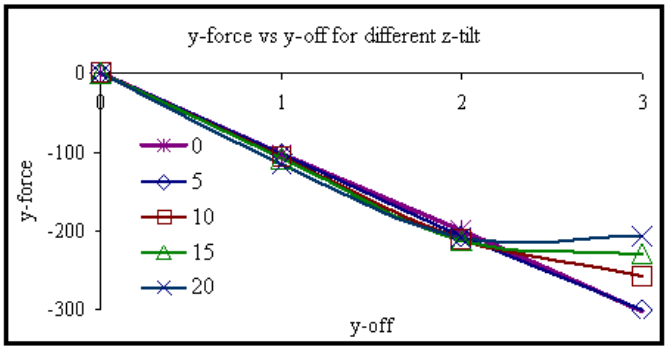

Figure 20 Comparison of y-force vs. y-offset at 100V for different tilt in z-axis.

The force measurements are not highly sensitive with varied tilts in z-axis for small y-offsets. The variation is due to increase in the edge length of the top plate across the junction of the electrodes as illustrated in Figure 21.

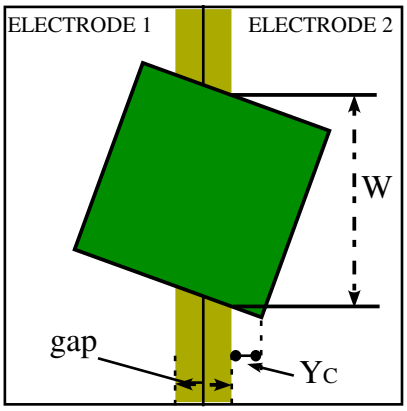

W - Edge Length of the top plate
Yc - Critical y-offset beyond which
edge length (W) varies with y-offset

Figure 21 Illustration to predict edge length with the tilt in z-axis.

The term Yc in Figure 21 is to denote the distance from the edge of the gap to the corner of the top plate. The value of Yc varies depending on the tilt in the z-axis. When the top plate has a *z-tilt* of value θ, then the value of Yc can be calculated as

$$Y_c = \left(\left[\frac{L}{2 * Cos45} \right] * Cos(45 + \theta) \right) - gap/2$$

Equation 6 Predition of critical y-offset based on *z-tilt*.

Where Yc is the critical y-offset for tilt θ in z-axis and gap is the distance between the two electrodes. When a part with the *z-tilt* is offset from the mean position the edge length (W) of the top plate over the electrode can be determined by

$$W = L / Cos\,\theta$$

Equation 7 Prediction of edge length of the top plate when y-offset is below the critical y-offset value.

Where L is the side length of the top plate and θ is the *z-tilt*. This value (W) is a constant till an offset value of Yc (determined earlier). Once the offset exceeds the value of Yc, the edge length varies with offset and the value of the edge length in such a case is determined from

$$W = \left[\frac{L * Sin\theta - \left(y_{off} - Yc\right)}{Sin\theta * Cos\theta}\right]$$

Equation 8 Prediction of edge length of the top plate when y-offset exceeds critical y-offset value.

Where

θ	–	value of tilt in z-axis
y_{off}	-	actual offset defined to displace the top plate (m)
Y_c	-	Critical offset value for a particular tilt (m)
Gap	-	gap between electrodes (m)

The surface energies required for the calculation were obtained from the Surface Evolver prediction based on the area of electrode over each pad. Once these values are calculated, y-force can be calculated from

$$\left[(\gamma_L - \gamma_R) * W\right] = F_Y$$

Equation 9 y-force calculation based on surface energy difference and edge length variation.

γ_L	-	Surface tension on the left pad (N/m^2)
γ_R	-	Surface tension on the right pad (N/m^2)
W	-	Edge length of the cover plate (m)
F_Y	-	Force in the y-direction (N)

It is necessary to align the part within 5 ° tilt to z-plane to limit the variation to 3% of the measured value, however for highly precise results it is recommended to ensure alignment within 1 ° error thereby ensuring approximately the force values to vary within 0.3% of the actual value.

In order to compare the force results from Surface Evolver predictions with those of hand calculations 20 ° *z-tilt* is chosen at a random. The results for force in the y-direction are predicted and compared with that of the results of Surface Evolver as shown in Figure 22. This procedure captures the expected variation at large displacements.

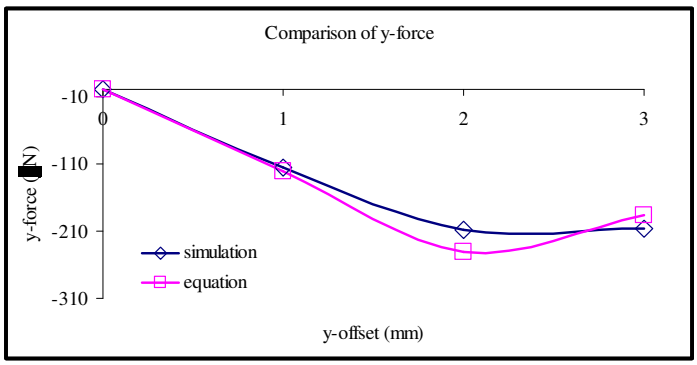

Figure 22 Comparison of simulation results and predicted results using equation for y-force vs. y-offset at 100V.

4.3.1.2 X - Tilt

Analysis was done with 0 ° tilt in the y and z-direction while the tilt in the x-axis is increased in steps and forces were analyzed for different y-offsets and a constant 100 V across the electrodes.

Even minute tilt in the x-axis causes greater variation in the measured force values. A 0.5 ° tilt in the x-axis displaces the part with a force of approximately 90μN at 0mm y-offset. Hence theoretically, the tilt in the x-axis has to be maintained at 0 ° tilt in order to obtain accurate forces due to electrowetting.

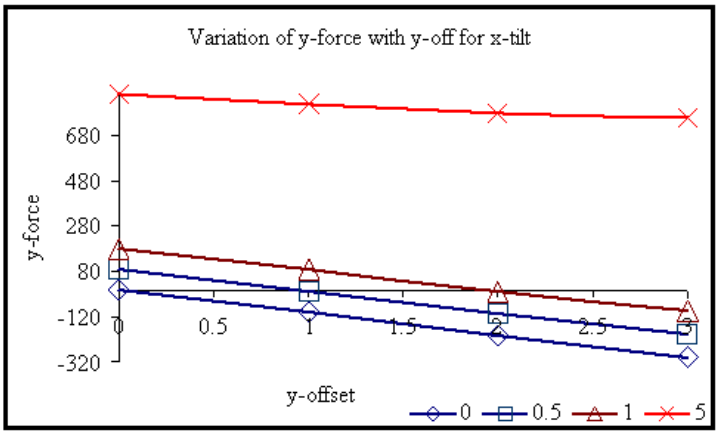

Figure 23 Comparison of y-force vs. y-offset at 100V for different tilt in x-axis.

Table 1 Comparison of best line fits for perfect alignment with those with different values of *x-tilt*.

X-tilt	Slope	Intercept	Slope Error
0	100.13	0.7376	NA
0.5	96.9	89.9	3.2%
1	91.4	178.9	8.7%
5	34.4	852.6	65.6%

However, the rate of change of force with offset is less sensitive to the *x-tilt* errors. From the graph shown in Figure 23, the slope of the results looks to be similar. Table 1 compares the best fit lines for perfect alignment to those with 0.5 °, 1 °, and 5 ° tilt in the x-axis.

For 0.5 degree tilt, the slope error is 3.2%. Possible methodologies can be derived to predict the tilt errors by detecting offset, however it would be preferred to minimize the tilt errors as the force measurements prove to be highly sensitive to minute tilt errors in the x-axis.

4.3.1.3 Y - Tilt

Analysis towards sensitivity of measurements with tilt in y-axis was done at 100V applied voltage. The tilt values of y-axis were increased in steps while the part was accurately aligned to x and z axis (0 º tilt). The resulting y-forces are shown in Figure 24. The y-force is very sensitive to *y-tilt*, but less sensitive than to *x-tilt*. The best fit line of perfect alignment condition is compared with those with 0.5, 1 and 5 degree tilt in y-axis in Table 2.

Table 2 Comparison of best line fits of those for perfect alignment with those with different values of *y-tilt.*

Y-tilt	Slope	Intercept	Slope Error
0	100.13	0.7376	NA
0.5	100.02	9.5221	0.109%
1	99.864	19.085	0.265%
5	93.658	131.89	6.46%

The alignment of the part along the y-axis is very important for consistent force measurements. Similar to those variations in the x-axis, 0.5 º tilt in the y-axis could offset a part with approximately 10μN of force in positive direction of the y-axis when at 0mm y-offset. However, the slope of the force change with offset varies just 1% for this tilt so that the error is less significant at higher offsets.

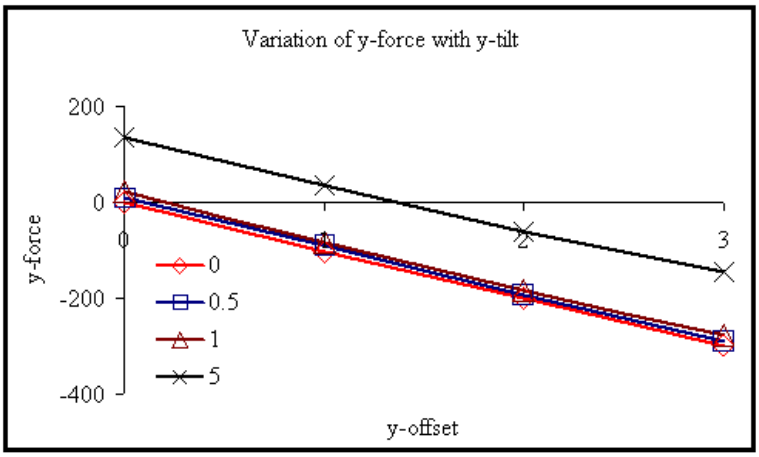

Figure 24 Comparison of y-force vs. y-offset at 100V for different tilt in y-axis.

From the analysis and comparison of the results from the Surface Evolver predictions, alignment requirements gain equal importance in both x and y axis for accurate force measurements.

4.3.2 Effects of Volume

A Liquid volume of 47µl was defined for the liquid on all simulations done and results compared. The drop volume is controlled by dispensing the drop with a micrometer syringe. The liquid volume is selected to provide a thin layer between the substrate and top plate. This ensures that the contact area on the substrate to closely approximate the area of the top plate. The micrometer syringe dispenses drop to approximately 1% accuracy. After dispensing and during the test, the drop volume may be decreased by evaporation. Therefore, it is important to consider the impact of drop volume variation.

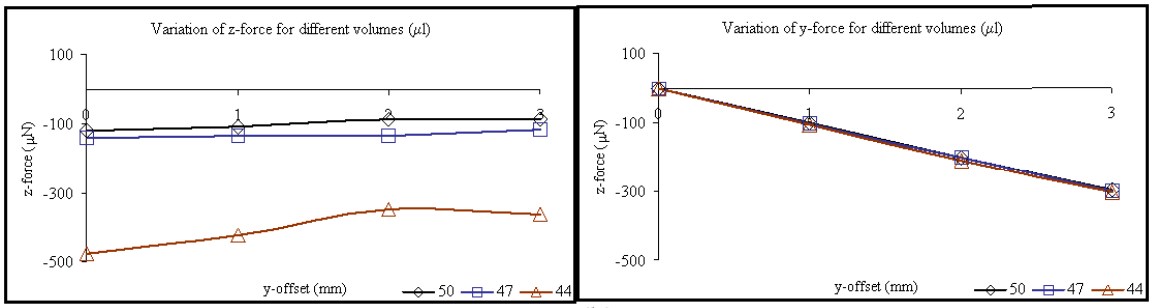

(a) (b)

Figure 25 Comparison of (a) z-force and (b) y-force vs. y-offset for different volume.

Analysis was run for three different drop volume levels at a constant electrode voltage of 100 V as summarized in Figure 25. While change of volume does not affect force measurements in the lateral direction, it has great significance when normal force measurements are considered. The variations according to the results show approximately 18% decrease from the actual force measurements for a 3µl increase from the actual volume, while a 3µl decrease has great influence on force measurements to increase by a factor of 100. Thus volume needs high control and consistency between measurements in order to compare z-force magnitudes. However, if the analysis is based on y-forces, then volume control is not critical.

4.4 Conclusions

The Surface Evolver model was used to find the electrowetting force measurements under a predetermined condition and analyzed for variations in these measurement values for changes in critical parameters. The range of variation is specified by comparing hand calculation and Surface Evolver prediction and the critical parameters to be controlled while measurements are taken. The tilt in the x-axis is found to produce high variations followed by *y-tilt*. *Z-tilt* introduce lesser variation compared to that of x and *y-tilt*. Volume had very negligible effect in the lateral force measurement and hence

volume is not a critical factor when lateral forces are considered. This analysis helps to predetermine the variation in the force measurements that might occur with possible reasons to support them. Since tilt causes the maximum possible variation from the actual value of electrowetting forces, one possible solution can be to align the part using the substrate surface as a fixture in itself so that the part is aligned parallel when compared to the substrate so as to avoid measurement errors.

CHAPTER 5 CONCLUSION AND FUTURE WORK

Capillary forces have vast potential at the micro and nano scale applications. This work generated novel techniques to measure these capillary forces in two important applications and proved that optimization of these forces based on the proposed technique provides great potential in the field. By optimizing these forces in the applications detailed in this thesis, there are high possibilities of these processes to meet commercial requirements.

5.1 Self Assembly

Self assembly methods have the potential to achieve fast, parallel, low cost assembly of micro and nano-components. However, the accuracy of the current assembly methods is limited by the ability to control the process variables. This work has drawn from techniques employed to achieve accurate positioning in macro-scale assembly and applied them to the case of capillary self assembly. Analysis of self assembly systems in the typical case and the proposed case are done. Critical force optimization and variations in the critical force with liquid volumes are also detailed. This analysis demonstrates that a modified capillary self assembly method based on this approach can reduce sensitivity of component positioning to process variation through a force-closure method. In the ideal case, the accuracy of the self assembly parts is only a function of the accuracy of a rigid alignment feature. Under this system, assembly bonds should be designed to ensure

that under expected variations, the preload force remains greater than the expected disturbance forces. Simple models are presented to provide adequate estimates of these forces as an aid in the component design. This dramatically simplifies the challenge of developing a robust, high yield process that can achieve high accuracy placement of microscale parts.

Future work will characterize the sources and magnitude of variation. One significant source of variation is in the volume of the assembly fluid. The magnitude of this variation for the common "dip coating" procedure would be measured. These measurements will be applied to the models developed in Chapter 3 to better assess their ability to maintain accurate positioning under uncertainty. This method will also be extended to self assembly processes based on other assembly forces.

The analytical methods developed in this work must be tested experimentally. The parts will be fabricated by evaporating chrome and copper to a plain silicon wafer and dicing them to the required part dimensions. Alignment feature as detailed in the proposed technique would be fabricated by standard photolithography technique using SU-8 2150 photoresist and the binding sites would be patterned by evaporating chrome and copper for the required patterns through lift-off technique. The optimization of liquid volume by dip coating procedure detailed earlier can be a good start to decide on the height on the alignment feature required. Based on these results, characterization of photoresist SU-8 2150 would be done based on the height of the alignment feature required for the proposed technique.

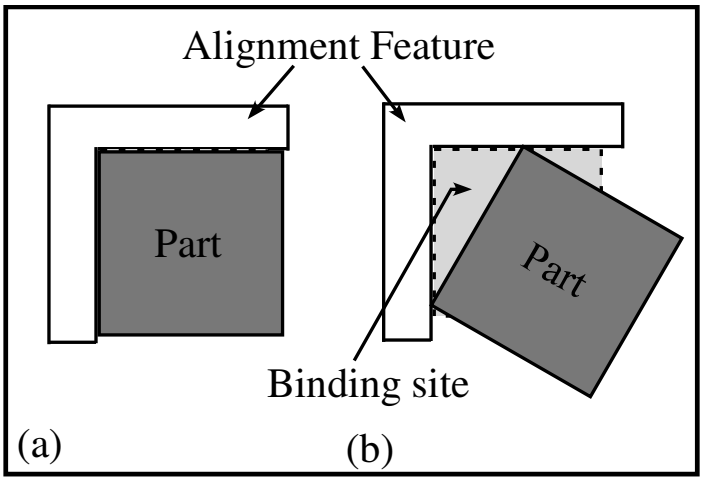

Figure 26 Schematic illustration of wedging in the proposed self assembly model.

These models have analyzed parts in or near the assembly position as illustrated in Figure 26(a). However, during assembly, the parts may contact in other locations. Ideally, the liquid will create a continuous driving force towards assembly. However, under some conditions, the parts will contact the barriers as illustrated in Figure 26(b). "Wedging" could occur if capillary forces that promote assembly cannot overcome the frictional forces against the alignment feature as shown in Figure 26(b). Future work will characterize those forces that are responsible for wedging and will identify the part dimensions and friction ranges in which wedging may occurs. Based on those results, a solution can be developed. This problem will be characterized by determining the actual force/agitation required to overcome wedging issue in the proposed assembly technique.

5.2 Electrowetting Force Variation

Electrowetting is a promising technique for droplet transport, mixing and control in applications related to microfluidics. There are numerous applications with those including micro optical switching devices and micro fluidic pumps that give tremendous opportunities to microfluidics. From many previous research works, the potential of

electrowetting was proven but proper knowledge and prediction of the force variations will enable efficient control of droplet by electrowetting. Further, process improvement is possible by optimizing the force induced. These forces were measured by Crane et al. in [22] using a nanoindenter.

This analysis validated the measurement accuracy from the nanoindenter. Further, results are obtained for those variations in the measurement system due to possible error sources with those including part tilt and excess liquid volumes. These results are compared to identify the range of measurement variations and their sensitivity expected under such conditions. Current analysis is done based on certain assumptions with those including assuming the part as a rigid body and thus neglecting the deflections induced in them. In future, the part defined in the analysis could be analyzed in Ansys by defining the force equivalent to that induced by the liquid along the edges of the part and apply pressure through the area beneath the part with those values from the Surface Evolver to predict the deflection and force variations produced by these deflections.

REFERENCES

[1] K. P. Ellis., “Optimizing the performance of a surface mount placement machine”. IEEE transactions on electronics packaging manufacturing 24(3), pp. 160.

[2] A. Singh, D. A. Horsley, M. B. Cohn, A. P. Pisano and R. T. Howe, "Batch transfer of microstructures using flip-chip solder bonding," J Microelectromech Syst, vol. 8, pp. 27-33, 03. 1999.

[3] K. Verma, M. A. Hadley and J. S. Smith, "Fluidic self-assembly of silicon microstructures", 1995.

[4] K. F. Bohringer, U. Srinivasan and R. T. Howe, "Modeling of capillary forces and binding sites for fluidic self-assembly”, 14th IEEE International Conference on Micro Electro Mechanical Systems (MEMS 2001), Jan 21-25 2001, 2001, pp. 369-374.

[5] U. Srinivasan, D. Liepmann and R. T. Howe, "Microstructure to substrate self-assembly using capillary forces”, J Microelectromech Syst, vol. 10, pp. 17-24, 2001.

[6] G. M. Whitesides and B. Grzybowski, “Self-assembly at all scales", Science, vol. 295, pp. 2418-2421, MAR 29. 2002.

[7] A. Greiner, J. Lienemann, J. G. Korvink, X. Xiong, Y. Hanein and K. F. Bohringer, "Capillary forces in micro-fluidic self-assembly", 2002, International Conference on Modeling and Simulation of Microsystems - MSM 2002, Apr 21-25 2002, 2002, pp. 198-201.

[8] J. Tien, A. Terfort and G. M. Whitesides, "Microfabrication through electrostatic self-assembly", Langmuir, vol. 13, pp. 5349-5355, OCT 1. 1997.

[9] S. Shet, V. R. Mehta, A. T. Fiory, M. P. Lepselter and N. M. Ravindra, "The magnetic field-assisted assembly of nanoscale semiconductor devices: A new technique", JOM, vol. 56, pp. 32-34, OCT. 2004.

[10] J. C. Love, A. R. Urbach, M. G. Prentiss and G. M. Whitesides, "Three-dimensional self-assembly of metallic rods with submicron diameters using magnetic interactions", J. Am. Chem. Soc., vol. 125, pp. 12696-12697, OCT 22. 2003.

[11] J. Lienemann, A. Greiner and J. G. Korvink, "Modeling, Simulation, and Experimentation of a Promising New Packaging Technology: Parallel Fluidic Self-Assembly of Microdevices".

[12] S. A. Stauth and B. A. Parviz, "Modeling of fluidic self-assembly for integration of silicon components on plastic", 19th IEEE International Conference on Micro Electro Mechanical Systems, 2006, pp. 194-197.

[13] Xiaorong Xiong, Sheng-Hsiung Liang and K. F. Bohringer, "Geometric binding site design for surface-tension driven self-assembly", IEEE International Conference on Robotics and Automation, 26 April, 2004, pp. 1141-8.

[14] J. Fang and K. F. Bohringer, "Parallel micro component-to-substrate assembly with controlled poses and high surface coverage", J Micromech Microengineering, vol. 16, pp. 721-730, APR. 2006.

[15] J. Lienemann, A. Greiner and J. G. , Korvink, "Modeling, Simulation, and optimization of electrowetting", IEEE Transactions on Computer-Aided Design of Integrated Circuits and Systems, vol. 25, pp. 234-47, 02. 2006.

[16] K. Brakke, "The Surface Evolver", vol. 2007, September 13, 2005. 2005.

[17] F. Mugele. (2005, “Electrowetting: From basics to applications”, Journal of physics. Condensed matter 17(28), pp. R705.

[18] Chang-Jin Kim, “http://www.research.ucla.edu/tech/ucla00-270.htm”.

[19] J. C. Berg, "Wettability”, Basel and Hong Kong: Marcel Dekker Inc., 1993.

[20] J. L. Lin, G. B. Lee, Y. H. Chang and K. Y. Lien, "Model description of contact angles in electrowetting on dielectric layers", Langmuir, vol. 22, pp. 484-489, JAN 3. 2006.

[21] S. Walker and B. Shapiro, "Modeling the fluid dynamics of Electrowetting on Dielectric (EWOD)", 2004 NSTI Nanotechnology Conference and Trade show - NSTI Nanotech 2004, pp. 391-394.

[22] Nathan Brad Crane, Alex A Volinsky, Vivek Ramadoss, Michael Nellis, Pradeep Mishra, Xiaolu Pang, "Analysis and Measurement of Forces in an Electrowetting-Driven Oscillator", 2007.

[23] John A. Pelesko, “Self assembly, the Science of Things that Put Themselves Together”, Taylor & Francis Group, 2007.

[24] W. Zheng, P. Buhlmann and H. O. Jacobs, "Sequential shape-and-solder-directed self-assembly of functional microsystems", Proc. Natl. Acad. Sci. U. S. A., vol. 101, pp. 12814-12817, AUG 31. 2004.

[25] A. H. Cannon, Y. M. Hua, C. L. Henderson and W. P. King, "Self-assembly for three-dimensional integration of functional electrical components", J Micromech Microengineering, vol. 15, pp. 2172-2178, NOV. 2005.

[26] D. H. Gracias., “Forming electrical networks in three dimensions by self-assembly”, Science 289(5482), pp. 1170.

[27] X. R. Xiong, Y. Hanein, J. D. Fang, Y. B. Wang, W. H. Wang, D. T. Schwartz and K. F. Bohringer, "Controlled multibatch self-assembly of microdevices", J Microelectromech Syst, vol. 12, pp. 117-127, APR. 2003.

[28] V. Jairazbhoy, "Prediction of equilibrium shapes and pedestal heights of solder joints for leadless chip components", IEEE Transactions on Components, Packaging, and Manufacturing Technology. Part A, vol. 19, pp. 224, 1996.

[29] K. L. Scott, T. Hirano, H. Yang, R. T. Howe and A. M. Niknejad, "High-performance inductors using capillary based fluidic self-assembly", J Microelectromech Syst, vol. 13, pp. 300-309, APR. 2004.

[30] W. Zheng and H. O. Jacobs, "Self-assembly process to integrate and connect semiconductor dies on surfaces with single-angular orientation and contact-pad registration", Adv Mater, vol. 18, pp. 1387, JUN 6. 2006.

[31] H. J. Yeh and J. S. Smith, "Fluidic assembly for the integration of GaAs light-emitting diodes on Si substrates", IEEE Photon. Technol. Lett., vol. 6, pp. 706, 1994.

[32] U. Srinivasan, M. A. Helmbrecht, C. Rembe, R. S. Muller and R. T. Howe, "Fluidic self assembly of micromirrors onto microactuators using capillary forces", IEEE Journal of Selected Topics in Quantum Electronics, vol. 8, pp. 4-11,FEB. 2002.

[33] B. P. Singh, K. Onozawa, K. Yamanaka, T. Tojo and D. Ueda, "Novel high precision optoelectronic device fabrication technique using guided fluidic assembly", Optical Review, vol. 12, pp. 345-351, AUG. 2005.

[34] K. Harsh, "Modeling for solder self-assembled MEMS", Proceedings of SPIE--the International Society for Optical Engineering, vol. 3289, pp. 177, 1998.

[35] V. Cristini and Yung-Chieh Tan, "Theory and numerical simulation of droplet dynamics in complex flows - a review", Lab on a Chip, vol. 4, pp. 257-64, 2004.

[36] Y. Fouillet, D. Jary, A. G. Brachet, J. Berthier, R. Blervaque, L. Davous, J. M. Roux, J. L. Achard and C. Peponnet, "EWOD digital microfluidics for lab on a chip", 4th International Conference on Nanochannels, Microchannels and Minichannels, ICNMM2006, pp. 1255-1264, 2006.

[37] E. Baird, P. Young and K. Mohseni, "Electrostatic force calculation for an EWOD-actuated droplet", Microfluidics and Nanofluidics, vol. 3, pp. 635-644, 2007.

[38] S. W. Walker and B. Shapiro, "Modeling the fluid dynamics of Electrowetting on Dielectric (EWOD)", J Microelectromech Syst, vol. 15, pp. 986-1000, 2006.

[39] V. Peykov, A. Quinn and J. Ralston, "Electrowetting: a model for contact-angle saturation", Colloid & Polymer Science, vol. 278, pp. 789-93, 2000.

[40] J. Berthier, “Actuation potentials and capillary forces in Electrowetting based Microsystems”, Sensors and actuators. A, Physical 134(2), pp. 471.

[41] J. A. Thompson and R. S. Fearing, "Automating microassembly with ortho-tweezers and force sensing", Proceedings of RSJ/IEEE International Conference on Intelligent Robots and Systems, pp. 1327-34, 2001.

[42] A. Terfort, “Self-assembly of an operating electrical circuit based on shape complementarity and the hydrophobic effect”, Advanced materials 10(6), pp. 470, 1998.

[43] D. E. Whitney, “Mechanical Assemblies: Their Design, Manufacture, and Role in Product Development”, 1st ed.New York: Oxford University Press, pp. 517, 2004.

APPENDICES

Appendix A: Program to Support the Analysis of Capillary Forces

```
//program to automate the analysis

run_program.cmd

printf """>>> "x_loc.dat"

printf """>>> "y_loc.dat"

printf """>>> "z_loc.dat"

printf """>>> "x_rot.dat"

printf """>>> "y_rot.dat"

printf """>>> "z_rot.dat"

printf """>>> "xforce.dat"

printf """>>> "yforce.dat"

printf """>>> "zforce.dat"

printf """>>> "xphiforce.dat"

printf """>>> "yphiforce.dat"

printf """>>> "zphiforce.dat"

printf """>>> "totalenergy.dat"

printf """>>> "volume.dat"

printf """>>> "pressure.dat"

printf """>>> "ti_log.txt"
```

Appendix A (Continued)

```
// Postscript options
gridflag off ;
labelflag off ;
pscolorflag on;

tt :=0;
// g until glue has calmed down
cgl_TOL := 6e-8;
calm_glue :=
{
//printf "cgl: %15.15g -> ",total_energy >> "ti_log.txt";
conj_grad off; g10; conj_grad on;
g20;
do
{
cgl_old_e := total_energy;
g 10;
}
 while (abs((cgl_old_e-total_energy)/total_energy)>cgl_TOL);
printf "%15.15g -> %15.15g\n",cgl_old_e,total_energy >> "ti_log.txt";
};
```

Appendix A (Continued)

```
fz_TOL := 6e-9;
fz_movlim:=1e-6;
fz_maxit:=15;
find_zmin := // by Newton-Raphson
{
fz_it :=0;
do
{
fz_it += 1;
fz_old_CZ := z_loc;
fz_old_energy := total_energy; // save old values

calc_zf ; // calculate derivative
fz_hstr := dEdz;
fz_alpha := -dEdz/d2Edz2; // Newton

// Apply motion limit
if ( fz_alpha > 0 ) then fz_alpha:=minimum(fz_alpha,fz_movlim)
else fz_alpha:=maximum(fz_alpha,-fz_movlim);
```

Appendix A (Continued)

```
// Shift micropart

new_z_loc := fz_old_CZ + fz_alpha;

change_z_loc;

calm_glue;


// Backtracking scheme, if Newton failes

if ( total_energy>fz_old_energy) then

{

 fz_alpha := - fz_hstr *fz_alpha^2/(2*(total_energy-fz_hstr*fz_alpha-fz_old_energy));

new_z_loc := fz_old_CZ + fz_alpha;

change_z_loc; calm_glue;

};


printf "fz %g: z_loc: %10e, l: %10e, old_z_loc:%10e\n", fz_it ,z_loc,fz_alpha,fz_old_CZ
>> "ti_log.txt";

} while (abs(fz_old_CZ-z_loc)>fz_TOL) and (fz_it<fz_maxit);

};

fp_cgTOL := 0.8e-4; // angular tolerance

fp_nr_damping := 0.99; // Damping for Newton-Raphson

fp_backstep_damping:=0.5;

fp_movlim := 1;
```

Appendix A (Continued)

```
fp_maxit := 20;
find_phimin:= // using Newton's Method
{
fp_iter := 0;

do // while Sum Delta CfX,Y,ZgPHI > TOL
{
fp_iter += 1;
fp_CX_old := x_rot; // save x,k
fp_CY_old := y_rot;
fp_CZ_old := z_rot;
fp_old_energy := total_energy;

// get gradient
calc_phif ;
fp_g1 := dEdphix;
fp_g2 := dEdphiy;
fp_g3 := dEdphiz;

fp_a := d2Edphix2;
fp_b := d2Edphixy;
fp_c := d2Edphixz;
```

Appendix A (Continued)

```
fp_d := d2Edphiy2;

fp_e := d2Edphiyz;

fp_f := d2Edphiz2;


// invert Hessian

fp_idiv := -fp_c^2*fp_d + 2* fp_b*fp_c*fp_e - fp_a*fp_e^2 - fp_b^2* fp_f + fp_a*fp_d*
fp_f ;

fp_ai := (-fp_e^2 + fp_d* fp_f )/ fp_idiv ;

fp_bi := ( fp_c*fp_e - fp_b* fp_f )/ fp_idiv ;

fp_ci := (-fp_c*fp_d + fp_b*fp_e )/ fp_idiv ;

fp_di := (-fp_c ^2 + fp_a* fp_f )/ fp_idiv ;

fp_ei := ( fp_b*fp_c - fp_a*fp_e )/ fp_idiv ;

fp_fi := (-fp_b^2 + fp_a*fp_d )/ fp_idiv ;


// Newton step

fp_step := ( fp_g1* fp_ai + fp_g2* fp_bi + fp_g3* fp_ci )*fp_nr_damping;

if fp_step>0 then fp_step := minimum(fp_step,fp_movlim)

else fp_step := maximum(fp_step,-fp_movlim);

new_x_rot := x_rot - fp_step;

fp_step := ( fp_g1* fp_bi + fp_g2* fp_di + fp_g3* fp_ei )*fp_nr_damping;

if fp_step>0 then fp_step := minimum(fp_step,fp_movlim)

else fp_step := maximum(fp_step,-fp_movlim);
```

Appendix A (Continued)

```
new_y_rot := y_rot - fp_step;

fp_step := ( fp_g1* fp_ci + fp_g2* fp_ei + fp_g3* fp_fi )*fp_nr_damping;


if fp_step>0 then fp_step := minimum(fp_step,fp_movlim)

else fp_step := maximum(fp_step,-fp_movlim);

new_z_rot := z_rot - fp_step;

change_rot; calm_glue;


//printf "fp%g after Newton: x_rot: %10e, y_rot: %10e, z_rot: %10e, E: %10e\n", fp_iter
,x_rot,y_rot,z_rot,total_energy >> "ti_log.txt";


if ( total_energy>fp_old_energy) then

{

 new_x_rot := fp_CX_old - fp_backstep_damping* (x_rot-fp_CX_old);

new_y_rot := fp_CY_old - fp_backstep_damping* (y_rot-fp_CY_old);

new_z_rot := fp_CZ_old - fp_backstep_damping* (z_rot-fp_CZ_old);

change_rot; calm_glue;

printf "fp_%g Newton failed: x_rot: %10e, y_rot: %10e, z_rot: %10e, E: %10e\n", fp_iter
,x_rot,y_rot,z_rot,total_energy >> "ti_log.txt";

};
```

Appendix A (Continued)

```
} while ( abs(fp_CX_old-x_rot)+ abs(fp_CY_old-y_rot)+ abs(fp_CZ_old-z_rot) > fp_cgTOL) and (fp_iter<fp_maxit);

};


ti_CXstep := 0; // will be set later

ti_CYstep := 0;

ti_iter:=0;

ti_maxiter:=30;

ti :=

{


tt +=1;

printf "********** time: %g **********\n",tt;

printf "********** time: %g **********\n",tt >> "ti_log.txt";


// ------ lateral shift and stiffening effect -----------

do {

find_zmin;

find_phimin;

find_zmin;

ti_iter+=1;

} while (abs(fz_old_CZ-z_loc)>fz_TOL and (ti_iter<ti_maxiter));
```

Appendix A (Continued)

```
calc_xf ; calc_yf ; calc_zf ;

// write out data

printf "ti: dEdx: %10e, dEdy: %10e, dEdz: %10e\n",dEdx,dEdy,dEdz >> "ti_log.txt";

printf "ti: x_loc: %10e, y_loc: %10e, z_loc: %10e\n",x_loc,y_loc,z_loc >> "ti_log.txt";

printf "%17.15g\n", x_loc >> "x_loc.dat";

printf "%17.15g\n", y_loc >> "y_loc.dat";

printf "%17.15g\n", z_loc >> "z_loc.dat";

printf "%17.15g\n", x_rot >> "x_rot.dat";

printf "%17.15g\n", y_rot >> "y_rot.dat";

printf "%17.15g\n", z_rot >> "z_rot.dat";

printf "%17.15g\n", xforce >> "xforce.dat";

printf "%17.15g\n", yforce >> "yforce.dat";

printf "%17.15g\n", zforce >> "zforce.dat";

printf "%17.15g\n", -dEdphix >> "xphiforce.dat";

printf "%17.15g\n", -dEdphiy >> "yphiforce.dat";

printf "%17.15g\n", -dEdphiz >> "zphiforce.dat";

printf "%17.15g\n", total_energy >> "totalenergy.dat";

printf "%17.15g\n", body[1].volume >> "volume.dat";

printf "%17.15g\n", body[1].pressure >> "pressure.dat";

printf "%17.15g %17.15g %17.15g\n", x_loc,y_loc,total_energy >> "X-Y-E.dat";
```

Appendix A (Continued)

```
// ------ lateral shift --------------------------------
new_x_loc := x_loc + ti_CXstep; change_x_loc;
new_y_loc := y_loc + ti_CYstep; change_y_loc;
g 30;

// vertex averaging and equiangulation
V; u; V;
calm_glue;
};

calc_force.cmd
calc_xf := { f_dx := pad_xdim1/1000; // small shift
new_x_loc := x_loc + f_dx; change_x_loc;
energy_hi := total_energy - body[1].pressure*(body[1].volume-body[1].target);
new_x_loc := x_loc - 2*f_dx; change_x_loc;
energy_lo := total_energy - body[1].pressure*(body[1].volume-body[1].target);
new_x_loc := x_loc + f_dx; change_x_loc;
energy_mid := total_energy - body[1].pressure*(body[1].volume-body[1].target);
dEdx := (energy_hi - energy_lo)/(2*f_dx );
d2Edx2 :=( (energy_hi - 2*energy_mid + energy_lo)/(f_dx)^2);
xforce := -dEdx;
```

Appendix A (Continued)

```
//printf "xforce: %17.15gnn",xforce;
}

calc_yf := { f_dy := pad_ydim1/1000; // small shift
new_y_loc := y_loc + f_dy; change_y_loc;
energy_hi := total_energy - body[1].pressure*(body[1].volume-body[1].target);
new_y_loc := y_loc - 2*f_dy; change_y_loc;
energy_lo := total_energy - body[1].pressure*(body[1].volume-body[1].target);
new_y_loc := y_loc + f_dy; change_y_loc;
energy_mid := total_energy - body[1].pressure*(body[1].volume-body[1].target);
dEdy := (energy_hi - energy_lo)/(2*f_dy );
d2Edy2 := ((energy_hi - 2*energy_mid + energy_lo)/(f_dy)^2);
yforce := -dEdy;
//printf "yforce: %17.15gnn",yforce;
}

calc_zf := {  f_dz := ( z_loc-part_zdim/2)/1000; // small shift
new_z_loc := z_loc + f_dz; change_z_loc;
energy_hi := total_energy - body[1].pressure*(body[1].volume-body[1].target);
new_z_loc := z_loc - 2*f_dz; change_z_loc;
energy_lo := total_energy - body[1].pressure*(body[1].volume-body[1].target);
new_z_loc := z_loc + f_dz; change_z_loc;
```

Appendix A (Continued)

```
energy_mid := total_energy - body[1].pressure*(body[1].volume-body[1].target);
dEdz := (energy_hi - energy_lo)/(2*f_dz );
d2Edz2 := ((energy_hi - 2*energy_mid + energy_lo)/(f_dz)^2);
zforce := -dEdz;
//printf "zforce: %17.15gnn",zforce;
}



calc_phif :=
{
 f_dpx := 0.0005; f_dpy := 0.0005; f_dpz:=0.0005;
cp_x_rot:=x_rot; cp_y_rot:=y_rot; cp_z_rot:=z_rot;
new_x_rot := cp_x_rot+f_dpx; change_rot;
pxenergy_hi := total_energy - body[1].pressure*(body[1].volume-body[1].target);
new_y_rot := cp_y_rot+f_dpy; change_rot;
pxyenergy_hi := total_energy - body[1].pressure*(body[1].volume-body[1].target);
new_x_rot := cp_x_rot; change_rot;
pyenergy_hi := total_energy - body[1].pressure*(body[1].volume-body[1].target);
new_x_rot := cp_x_rot-f_dpx; new_y_rot := cp_y_rot; change_rot;
pxenergy_lo := total_energy - body[1].pressure*(body[1].volume-body[1].target);
new_y_rot := cp_y_rot-f_dpy; new_x_rot := cp_x_rot; change_rot;
pyenergy_lo := total_energy - body[1].pressure*(body[1].volume-body[1].target);
```

Appendix A (Continued)

```
new_y_rot := cp_y_rot; new_z_rot := cp_z_rot + f_dpz; change_rot;
pzenergy_hi := total_energy - body[1].pressure*(body[1].volume-body[1].target);
new_x_rot := cp_x_rot + f_dpx; change_rot;
pxzenergy_hi := total_energy - body[1].pressure*(body[1].volume-body[1].target);
new_x_rot := cp_x_rot; new_y_rot := cp_y_rot+f_dpy; change_rot;
pyzenergy_hi := total_energy - body[1].pressure*(body[1].volume-body[1].target);
new_y_rot := cp_y_rot; new_z_rot := cp_z_rot-f_dpz; change_rot;
pzenergy_lo := total_energy - body[1].pressure*(body[1].volume-body[1].target);
new_x_rot := cp_x_rot; new_y_rot := cp_y_rot; new_z_rot := cp_z_rot; change_rot;
energy_mid := total_energy - body[1].pressure*(body[1].volume-body[1].target);

dEdphix := (pxenergy_hi-pxenergy_lo)/(2*f_dpx);
dEdphiy := (pyenergy_hi-pyenergy_lo)/(2*f_dpy);
dEdphiz := (pzenergy_hi-pzenergy_lo)/(2*f_dpz);
d2Edphix2 := ((pxenergy_hi - 2*energy_mid + pxenergy_lo)/(f_dpx)^2);
d2Edphiy2 := ((pyenergy_hi - 2*energy_mid + pyenergy_lo)/(f_dpy)^2);
d2Edphiz2 := ((pzenergy_hi - 2*energy_mid + pzenergy_lo)/(f_dpz)^2);
d2Edphixy := (pxyenergy_hi-pxenergy_hi-pyenergy_hi+energy_mid)/(f_dpx*f_dpy);
d2Edphixz := (pxzenergy_hi-pxenergy_hi-pzenergy_hi+energy_mid)/(f_dpx*f_dpz);
d2Edphiyz := (pyzenergy_hi-pyenergy_hi-pzenergy_hi+energy_mid)/(f_dpy*f_dpz);
};
```

Appendix A (Continued)

```
read "calcinertia.cmd"

calc_planes.cmd

calc_normals:=

{

c_sx := sin(x_rot*pi/180);

c_sy := sin(y_rot*pi/180);

c_sz := sin(z_rot*pi/180);

c_cx := cos(x_rot*pi/180);

c_cy := cos(y_rot*pi/180);

c_cz := cos(z_rot*pi/180);

// multiply with R^-1 = R^T

c_Axp1 := (c_cy*c_cz);

c_Axp2 := (c_sx*c_sy*c_cz+c_cx*c_sz);

c_Axp3 := (-c_cx*c_sy*c_cz+c_sx*c_sz);

c_Axn1 := (-c_cy*c_cz);

c_Axn2 := (-(c_sx*c_sy*c_cz+c_cx*c_sz));

c_Axn3 := (-(-c_cx*c_sy*c_cz+c_sx*c_sz));

c_Ayp1 := (-c_cy*c_sz);

c_Ayp2 := (c_cx*c_cz-c_sx*c_sy*c_sz);

c_Ayp3 := (c_sx*c_cz+c_cx*c_sy*c_sz);

c_Ayn1 := (c_cy*c_sz);
```

Appendix A (Continued)

```
c_Ayn2 := (-(c_cx*c_cz-c_sx*c_sy*c_sz));

c_Ayn3 := (-(c_sx*c_cz+c_cx*c_sy*c_sz));

c_Azp1 := c_sy;

c_Azp2 := (-c_cy*c_sx);

c_Azp3 := (c_cx*c_cy);

c_Azn1 := (-c_sy);

c_Azn2 := (c_cy*c_sx);

c_Azn3 := (-c_cx*c_cy);

c_Pxp1 := x_loc + c_Axp1 * part_xdim/2;

c_Pxp2 := y_loc + c_Axp2 * part_xdim/2;

c_Pxp3 := z_loc + c_Axp3 * part_xdim/2;

c_Pxn1 := x_loc + c_Axn1 * part_xdim/2;

c_Pxn2 := y_loc + c_Axn2 * part_xdim/2;

c_Pxn3 := z_loc + c_Axn3 * part_xdim/2;

c_Pyp1 := x_loc + c_Ayp1 * part_ydim/2;

c_Pyp2 := y_loc + c_Ayp2 * part_ydim/2;

c_Pyp3 := z_loc + c_Ayp3 * part_ydim/2;

c_Pyn1 := x_loc + c_Ayn1 * part_ydim/2;

c_Pyn2 := y_loc + c_Ayn2 * part_ydim/2;

c_Pyn3 := z_loc + c_Ayn3 * part_ydim/2;

c_Pzp1 := x_loc + c_Azp1 * part_zdim/2;

c_Pzp2 := y_loc + c_Azp2 * part_zdim/2;
```

Appendix A (Continued)

```
c_Pzp3 := z_loc + c_Azp3 * part_zdim/2;

c_Pzn1 := x_loc + c_Azn1 * part_zdim/2;

c_Pzn2 := y_loc + c_Azn2 * part_zdim/2;

c_Pzn3 := z_loc + c_Azn3 * part_zdim/2;

}
```

change.cmd

```
define vertex attribute dist real

calc_dists :=

{

calc_normals;

foreach vertex vv do

{

if ( on_constraint 1 or on_constraint 2 or on_constraint 3 or on_constraint 4 or
on_constraint 5 or on_constraint 6 or on_constraint 13 )

then vv.dist := 1

else if fixed then vv.dist := 0

else

{

chipdist :=

maximum (0,c_Axn1*(x-c_Pxn1)+c_Axn2*(y-c_Pxn2)+c_Axn3*(z-c_Pxn3))+

maximum (0,c_Axp1*(x-c_Pxp1)+c_Axp2*(y-c_Pxp2)+c_Axp3*(z-c_Pxp3))+
```

Appendix A (Continued)

```
maximum (0,c_Ayn1*(x-c_Pyn1)+c_Ayn2*(y-c_Pyn2)+c_Ayn3*(z-c_Pxn3))+
maximum (0,c_Ayp1*(x-c_Pyp1)+c_Ayp2*(y-c_Pyp2)+c_Ayp3*(z-c_Pxp3))+
maximum (0,c_Azn1*(x-c_Pzn1)+c_Azn2*(y-c_Pzn2)+c_Azn3*(z-c_Pzn3))+
maximum (0,c_Azp1*(x-c_Pzp1)+c_Azp2*(y-c_Pzp2)+c_Azp3*(z-c_Pzp3));
if (( z+chipdist)!=0)
then vv.dist := z/(z+chipdist)
else vv. dist :=0.5;
}
};
}
// change x,y and z position of micropart
new_x_loc := x_loc
change_x_loc :=
{
calc_dists ;
change_dx := new_x_loc - x_loc; x_loc := new_x_loc;
set vertex x x+dist*change_dx;
recalc;
}
```

Appendix A (Continued)

```
new_y_loc := y_loc

change_y_loc :=

{

calc_dists ;

change_dy := new_y_loc - y_loc; y_loc := new_y_loc;

set vertex y y+dist*change_dy;

recalc;

}


new_z_loc := z_loc

change_z_loc :=

{

calc_dists ;

change_dz := new_z_loc - z_loc; z_loc := new_z_loc;

set vertex z z+dist*change_dz;

recalc;

}


// declare variables so that evolver knows them...

new_x_rot:=x_rot

new_y_rot:=y_rot

new_z_rot:=z_rot
```

Appendix A (Continued)

```
// rotate micropart
change_rot :=
{
 calc_dists ;
change_dxphi:= new_x_rot-x_rot;
x_rot := new_x_rot;
change_dyphi:= new_y_rot-y_rot;
y_rot := new_y_rot;
change_dzphi:= new_z_rot-z_rot;
z_rot := new_z_rot;

sdx := sin(change_dxphi*pi/180);
sdy := sin(change_dyphi*pi/180);
sdz := sin(change_dzphi*pi/180);
cdx := cos(change_dxphi*pi/180);
cdy := cos(change_dyphi*pi/180);
cdz := cos(change_dzphi*pi/180);

r11 := cdy*cdz;
r12 := -cdy*sdz;
r13 := sdy;
r21 := ( sdx*sdy*cdz+cdx*sdz);
```

Appendix A (Continued)

```
r22 := ( cdx*cdz-sdx*sdy*sdz);

r23 := -cdy*sdx;

r31 := (-cdx*sdy*cdz+sdx*sdz);

r32 := ( sdx*cdz+cdx*sdy*sdz);

r33 := cdx*cdy;


foreach vertex vv do

{

dx := x-x_loc; dy:=y-y_loc; dz:=z-z_loc;

set vv x x_loc + (1-dist) * dx + dist * ( r11*dx + r12*dy + r13*dz );

set vv y y_loc + (1-dist) * dy + dist * ( r21*dx + r22*dy + r23*dz );

set vv z z_loc + (1-dist) * dz + dist * ( r31*dx + r32*dy + r33*dz );

};

recalc;

}
```

Appendix A (Continued)

```
//program for analysis of self assembly
//Dimensions of part
parameter part_xdim = 900e-6 // [m]
parameter part_ydim =900e-6 // [m]
parameter part_zdim = 500e-6 // [m]

 //  reference location
parameter x_loc =0 // [m]
parameter y_loc = 0
parameter z_loc = 350e-6

 // to implement rotation
parameter z_rot = 0
parameter x_rot = 0
parameter y_rot = 0
parameter TMOBILITY = 1

// dimensions of pad (defined in two divisions to change dimensions along the midline
parameter pad_xdim1 = 900e-6 // [m]
parameter pad_xdim2 = 700e-6 // [m]
```

Appendix A (Continued)

```
parameter pad_ydim1 = 900e-6 // [m]

parameter pad_ydim2 =700e-6


// Physical properties

parameter TENSLW = 46e-3 // [J/m^2]

parameter TENSSW = 52e-3 // [J/m^2]

parameter TENSLS = 1e-3 // [J/m^2]


#define sx sin(x_rot*pi/180)

#define sy sin(y_rot*pi/180)

#define sz sin(z_rot*pi/180)

#define cx cos(x_rot*pi/180)

#define cy cos(y_rot*pi/180)

#define cz cos(z_rot*pi/180)


//vector representation of parts to enable translation and rotation along the local frame of reference

#define Axp1 (cy*cz) // r11

#define Axp2 (sx*sy*cz+cx*sz) // r21

#define Axp3 (-cx*sy*cz+sx*sz) // r31

#define Axn1 (-cy*cz) // -r11

#define Axn2 (-(sx*sy*cz+cx*sz)) // -r21
```

Appendix A (Continued)

```
#define Axn3 (-(-cx*sy*cz+sx*sz)) // -r31

#define Ayp1 (-cy*sz) // r12

#define Ayp2 (cx*cz-sx*sy*sz) // r22

#define Ayp3 (sx*cz+cx*sy*sz) // r32

#define Ayn1 (cy*sz) // -r12

#define Ayn2 (-(cx*cz-sx*sy*sz)) // -r22

#define Ayn3 (-(sx*cz+cx*sy*sz)) // -r32

#define Azp1 (sy) // r13

#define Azp2 (-cy*sx) // r23

#define Azp3 (cx*cy) // r33

#define Azn1 (-sy) // -r13

#define Azn2 (cy*sx) // -r23

#define Azn3 (-cx*cy) // -r33


// a reference point on the part

#define Pxp1 (x_loc + Axp1 * part_xdim/2)

#define Pxp2 (y_loc + Axp2 * part_xdim/2)

#define Pxp3 (z_loc + Axp3 * part_xdim/2)

#define Pxn1 (x_loc + Axn1 * part_xdim/2)

#define Pxn2 (y_loc + Axn2 * part_xdim/2)

#define Pxn3 (z_loc + Axn3 * part_xdim/2)

#define Pyp1 (x_loc + Ayp1 * part_ydim/2)
```

Appendix A (Continued)

```
#define Pyp2 (y_loc + Ayp2 * part_ydim/2)

#define Pyp3 (z_loc + Ayp3 * part_ydim/2)

#define Pyn1 (x_loc + Ayn1 * part_ydim/2)

#define Pyn2 (y_loc + Ayn2 * part_ydim/2)

#define Pyn3 (z_loc + Ayn3 * part_ydim/2)


#define Pzp1 (x_loc + Azp1 * part_zdim/2)

#define Pzp2 (y_loc + Azp2 * part_zdim/2)

#define Pzp3 (z_loc + Azp3 * part_zdim/2)

#define Pzn1 (x_loc + Azn1 * part_zdim/2)

#define Pzn2 (y_loc + Azn2 * part_zdim/2)

#define Pzn3 (z_loc + Azn3 * part_zdim/2)


// Constraints for part and pad (for display only)

constraint 1 // x+

formula: -(x - Pxp1) * Axp1 - (y - Pxp2) * Axp2 - (z - Pxp3) * Axp3 = 0

constraint 2 // x-

formula: -(x - Pxn1) * Axn1 - (y - Pxn2) * Axn2 - (z - Pxn3) * Axn3 = 0

constraint 3 // y+

formula: -(x - Pyp1) * Ayp1 - (y - Pyp2) * Ayp2 - (z - Pyp3) * Ayp3 = 0

constraint 4 // y-

formula: -(x - Pyn1) * Ayn1 - (y - Pyn2) * Ayn2 - (z - Pyn3) * Ayn3 = 0
```

Appendix A (Continued)

constraint 5 // z+

formula: -(x - Pzp1) * Azp1 - (y - Pzp2) * Azp2 - (z - Pzp3) * Azp3 = 0

constraint 6 // z-

formula: -(x - Pzn1) * Azn1 - (y - Pzn2) * Azn2 - (z - Pzn3) * Azn3 = 0

// Constraints for liquid (for calculation)

constraint 7 // keep glue above pad

formula: z = 0

energy:

e1: 0

e2: (TENSLS - TENSSW) *x

e3: 0

constraint 24 nonnegative // keep glue above substrate

formula: z

constraint 25 nonnegative // keep glue above substrate

formula: z-(z_loc-part_zdim/2)

constraint 13 // z- of chip , z+ of glue

formula: -(x - Pzn1) * Azn1 - (y - Pzn2) * Azn2 - (z - Pzn3) * Azn3 = 0

energy:

e1: (TENSLS-TENSSW) * (Azn3) * y

e2: (TENSLS-TENSSW) * (Azn1) * z

e3: (TENSLS-TENSSW) * (Azn2) * x

Appendix A (Continued)

content:

c1: 0

c2:-((Pzn3 + Azn1/Azn3 * Pzn1 + Azn2/Azn3 * (Pzn2 - y)) * x - Azn1/Azn3 * x^2/2)

c3: 0

// One-sided constraints for liquid on part.

constraint 14 nonpositive // keep glue within pos x bound

formula: (x - Pxp1) * Axp1 + (y - Pxp2) * Axp2 + (z - Pxp3) * Axp3

constraint 15 nonpositive // keep glue within neg x bound

formula: (x - Pxn1) * Axn1 + (y - Pxn2) * Axn2 + (z - Pxn3) * Axn3

constraint 16 nonpositive // keep glue within pos y bound

formula: (x - Pyp1) * Ayp1 + (y - Pyp2) * Ayp2 + (z - Pyp3) * Ayp3

constraint 17 nonpositive // keep glue within neg y bound

formula: (x - Pyn1) * Ayn1 + (y - Pyn2) * Ayn2 + (z - Pyn3) * Ayn3

// One-sided constraints for liquid on pad (substrate).

constraint 19 nonnegative //one-sided x-constraint on pad

formula: x-(0-pad_xdim1/2)

constraint 20 nonpositive //one-sided x-constraint on pad

formula: x-(0+pad_xdim2/2)

constraint 21 nonnegative //one-sided y-constraint on pad

formula: y-(0-pad_ydim1/2)

Appendix A (Continued)

constraint 22 nonpositive //one-sided y-constraint on pad

formula: y-(0+pad_ydim2/2)

//geometry definition starts here

vertices

//vertices of pad

1 -pad_xdim1/2 -pad_ydim1/2 -1e-7 fixed

2 pad_xdim2/2 -pad_ydim1/2 -1e-7 fixed

3 pad_xdim2/2 pad_ydim2/2 -1e-7 fixed

4 -pad_xdim1/2 pad_ydim2/2 -1e-7 fixed

//vertices of part

5 (x_loc-part_xdim/2) (y_loc-part_ydim/2) (z_loc-part_zdim/2) fixed constraint 13 14 15

6 (x_loc+part_xdim/2) (y_loc-part_ydim/2) (z_loc-part_zdim/2) fixed constraint 13 14 15

7 (x_loc+part_xdim/2) (y_loc+part_ydim/2) (z_loc-part_zdim/2) fixed constraint 13 14 15

8 (x_loc-part_xdim/2) (y_loc+part_ydim/2) (z_loc-part_zdim/2) fixed constraint 13 14 15

9 (x_loc-part_xdim/2) (y_loc-part_ydim/2) (z_loc+part_zdim/2) constraint 13 14 15

10 (x_loc+part_xdim/2) (y_loc-part_ydim/2) (z_loc+part_zdim/2) constraint 13 14 15

11 (x_loc+part_xdim/2) (y_loc+part_ydim/2) (z_loc+part_zdim/2) constraint 13 14 15

12 (x_loc-part_xdim/2) (y_loc+part_ydim/2) (z_loc+part_zdim/2) constraint 13 14 15

Appendix A (Continued)

//vertices of liquid

13 (x_loc-part_xdim/2) (y_loc-part_ydim/2) 0 constraint 7 19 20 21 22

14 (x_loc+part_xdim/2) (y_loc-part_ydim/2) 0 constraint 7 19 20 21 22

15 (x_loc+part_xdim/2) (y_loc+part_ydim/2) 0 constraint 7 19 20 21 22

16 (x_loc-part_xdim/2) (y_loc+part_ydim/2) 0 constraint 7 19 20 21 22

17 (x_loc-part_xdim/2) (y_loc-part_ydim/2) (z_loc-part_zdim/2) constraint 13 14 15 16 17

18 (x_loc+part_xdim/2) (y_loc-part_ydim/2) (z_loc-part_zdim/2) constraint 13 14 15 16 17

19 (x_loc+part_xdim/2) (y_loc+part_ydim/2) (z_loc-part_zdim/2) constraint 13 14 15 16 17

20 (x_loc-part_xdim/2) (y_loc+part_ydim/2) (z_loc-part_zdim/2) constraint 13 14 15 16 17

edges

1 1 2 no_refine fixed

2 2 3 no_refine fixed

3 3 4 no_refine fixed

4 4 1 no_refine fixed

Appendix A (Continued)

5 5 6 constraint 4 6 no_refine

6 6 7 constraint 1 6 no_refine

7 7 8 constraint 3 6 no_refine

8 8 5 constraint 2 6 no_refine

9 5 7 no_refine

10 9 10 constraint 4 5 no_refine

11 10 11 constraint 1 5 no_refine

12 11 12 constraint 3 5 no_refine

13 12 9 constraint 2 5 no_refine

14 9 11 no_refine

15 5 9 constraint 2 4 no_refine

16 6 10 constraint 1 4 no_refine

17 7 11 constraint 1 3 no_refine

18 8 12 constraint 2 3 no_refine

19 5 12 no_refine

20 6 9 no_refine

21 7 10 no_refine

22 8 11 no_refine

Appendix A (Continued)

23 13 14 constraint 7 19 20 21 22

24 14 15 constraint 7 19 20 21 22

25 15 16 constraint 7 19 20 21 22

26 16 13 constraint 7 19 20 21 22

27 17 18 constraint 13 17

28 18 19 constraint 13 14

29 19 20 constraint 13 16

30 20 17 constraint 13 15

31 13 17

32 14 18

33 15 19

34 16 20

faces

1 1 2 3 4 fixed no_refine color red

2 15 -13 -19 constraint 2 no_refine tension 0 color green

3 8 19 -18 constraint 2 no_refine tension 0 color green

4 6 21 -16 constraint 1 no_refine tension 0 color green

5 17 -11 -21 constraint 1 no_refine tension 0 color green

6 16 -10 -20 constraint 4 no_refine tension 0 color green

7 5 20 -15 constraint 4 no_refine tension 0 color green

Appendix A (Continued)

```
8 7 22 -17 constraint 3 no_refine tension 0 color green

9 18 -12 -22 constraint 3 no_refine tension 0 color green

10 -8 -7 -9 constraint 6 no_refine tension 0 color green

11 9 -6 -5 constraint 6 no_refine tension 0 color green

12 10 11 -14 constraint 5 no_refine tension 0 color green

13 12 13 14 constraint 5 no_refine tension 0 color green


14 26 31 -30 -34   tension TENSLW

15 24 33 -28 -32 tension TENSLW

16 23 32 -27 -31 tension TENSLW

17 25 34 -29 -33 tension TENSLW


bodies

1 14 15 16 17 volume (0.7*(pad_xdim1)*(pad_ydim1)*(z_loc-part_zdim/2))


//commads executed when running the program

read

//references to other cmd files related with this modeling

read "calcplanes.cmd"// normal vector calculations

read "change.cmd" // shift and rotate

read "calcforce.cmd"// calculate forces, torques and hessian
```

Appendix A (Continued)

```
target_tolerance := 1e-17 // because of small volume


//display liquid only
liquid_only := { set facet color clear where color == red or color == green}


read "run_program.cmd"
prepare:=
 { r;g10;r;g10;r;g20;
g10;
conj_grad;
g20;
};


logfile "selfassembly.log"
ti_angle:= 90;
quiet on;
showq;
prepare;


find_zmin;
new_x_loc := -40e-6*cos(ti_angle/180*pi); change_x_loc;
new_y_loc := -40e-6*sin(ti_angle/180*pi); change_y_loc;
```

Appendix A (Continued)

```
ti_CXstep := 20e-6*cos(ti_angle/180*pi);

ti_CYstep := 20e-6*sin(ti_angle/180*pi);

ti  6;

ti_CXstep *= -1;

ti_CYstep *= -1;

//ti 21;

quiet off ;
```

Appendix A (Continued)

```
//main program for electrowetting force analysis
//dimension of the plate
parameter PART_XDIM = 9e-3 // [m]
parameter PART_YDIM =9e-3 // [m]
parameter PART_ZDIM = 1e-3 // [m]

 // location of plate ( midpoint)
parameter X_LOC = 0// [m]
parameter Y_LOC = 3e-3
parameter Z_LOC = 1.08e-3

 // chip rotation
parameter Z_ROT = 1
parameter X_ROT = 0
parameter Y_ROT =0
parameter TMOBILITY = 1

// dimensions of pad
parameter PAD_XDIM = 20e-3 // [m]
parameter PAD_YDIM = 20e-3 // [m]
```

Appendix A (Continued)

```
// Physical properties
parameter TENSLW = 46e-3 // [J/m^2]
parameter TENSSW = 52e-3 // [J/m^2]
parameter TENSLS = 1e-3 // [J/m^2]

parameter height = Z_LOC-PART_ZDIM/2
parameter GAMMA_LV = 0.072
parameter E_r = 2.1
parameter E_o = 8.854e-12
parameter distance = 2.1e-6
parameter VOLTAGE = 100
parameter angle = 110
parameter topangle = 20
parameter GAP = 0.002

#define sx sin(X_ROT*pi/180)
#define sy sin(Y_ROT*pi/180)
#define sz sin(Z_ROT*pi/180)
#define cx cos(X_ROT*pi/180)
#define cy cos(Y_ROT*pi/180)
#define cz cos(Z_ROT*pi/180)
```

Appendix A (Continued)

```
// Nomenclature:
// x,y,z : face perpend. to x,y,z axis
// p: positive orientation , n: negative orientation
// 1,2,3: x,y and z component of vector
// Axp = R * (1,0,0), Axn = R * (-1,0,0)

#define Axp1 (cy*cz) // r11
#define Axp2 (sx*sy*cz+cx*sz) // r21
#define Axp3 (-cx*sy*cz+sx*sz) // r31
#define Axn1 (-cy*cz) // -r11
#define Axn2 (-(sx*sy*cz+cx*sz)) // -r21
#define Axn3 (-(-cx*sy*cz+sx*sz)) // -r31

// Ayp = R * (0,1,0), Ayn = R * (0,-1,0)
#define Ayp1 (-cy*sz) // r12
#define Ayp2 (cx*cz-sx*sy*sz) // r22
#define Ayp3 (sx*cz+cx*sy*sz) // r32
#define Ayn1 (cy*sz) // -r12
#define Ayn2 (-(cx*cz-sx*sy*sz)) // -r22
#define Ayn3 (-(sx*cz+cx*sy*sz)) // -r32
```

Appendix A (Continued)

```
// Azp = R * (0,0,1), Azn = R * (0,0,-1)

#define Azp1 (sy) // r13

#define Azp2 (-cy*sx) // r23

#define Azp3 (cx*cy) // r33

#define Azn1 (-sy) // -r13

#define Azn2 (cy*sx) // -r23

#define Azn3 (-cx*cy) // -r33


// a reference point on the face

#define Pxp1 (X_LOC + Axp1 * PART_XDIM/2)

#define Pxp2 (Y_LOC + Axp2 * PART_XDIM/2)

#define Pxp3 (Z_LOC + Axp3 * PART_XDIM/2)

#define Pxn1 (X_LOC + Axn1 * PART_XDIM/2)

#define Pxn2 (Y_LOC + Axn2 * PART_XDIM/2)

#define Pxn3 (Z_LOC + Axn3 * PART_XDIM/2)

#define Pyp1 (X_LOC + Ayp1 * PART_YDIM/2)

#define Pyp2 (Y_LOC + Ayp2 * PART_YDIM/2)

#define Pyp3 (Z_LOC + Ayp3 * PART_YDIM/2)

#define Pyn1 (X_LOC + Ayn1 * PART_YDIM/2)

#define Pyn2 (Y_LOC + Ayn2 * PART_YDIM/2)

#define Pyn3 (Z_LOC + Ayn3 * PART_YDIM/2)

#define Pzp1 (X_LOC + Azp1 * PART_ZDIM/2)
```

Appendix A (Continued)

```
#define Pzp2 (Y_LOC + Azp2 * PART_ZDIM/2)

#define Pzp3 (Z_LOC + Azp3 * PART_ZDIM/2)

#define Pzn1 (X_LOC + Azn1 * PART_ZDIM/2)

#define Pzn2 (Y_LOC + Azn2 * PART_ZDIM/2)

#define Pzn3 (Z_LOC + Azn3 * PART_ZDIM/2)


#define GAMMA_SL  (-GAMMA_LV*(cos(angle*pi/180)))  // virtual tension of facet
on plane

#define VOLT_LEFT (((Arightq.value+Aleftq.value)<1e-12)?
0.0:((Arightq.value/(Aleftq.value+Arightq.value))*VOLTAGE))

#define VOLT_RIGHT (((Arightq.value+Aleftq.value)<1e-12)?
0.0:((Aleftq.value/(Aleftq.value+Arightq.value))*VOLTAGE))

#define GAMMA_LEFT (GAMMA_SL-(((E_o*E_r)/(2*distance))*(VOLT_LEFT^2)))

#define GAMMA_RIGHT(GAMMA_SL-
(((E_o*E_r)/(2*distance))*(VOLT_RIGHT^2)))


#define left ((y<-GAP/2)? (y+GAP/2) : (0))

#define right ((y>GAP/2)? (y-GAP/2) : (0))

#define BTENS ((y<-GAP/2)?((GAMMA_LEFT*(y+GAP/2))-(GAP/2*GAMMA_SL)) :
(y>GAP/2)?((GAMMA_RIGHT*(y-GAP/2))+(GAP/2*GAMMA_SL)) :
(y*GAMMA_SL))
```

Appendix A (Continued)

```
#define UPPERT  (-cos(topangle*pi/180)*GAMMA_LV)


quantity Arightq INFO_ONLY method edge_vector_integral
vector_integrand:
  q1:  -(right)
  q2: 0
  q3: 0


quantity Aleftq INFO_ONLY method edge_vector_integral
vector_integrand:
  q1:  -(left)
  q2: 0
  q3: 0


// Constraints for chip and pad (display only)
constraint 1 // x+
formula: -(x - Pxp1) * Axp1 - (y - Pxp2) * Axp2 - (z - Pxp3) * Axp3 = 0
constraint 2 // x-
formula: -(x - Pxn1) * Axn1 - (y - Pxn2) * Axn2 - (z - Pxn3) * Axn3 = 0
constraint 3 // y+
formula: -(x - Pyp1) * Ayp1 - (y - Pyp2) * Ayp2 - (z - Pyp3) * Ayp3 = 0
```

Appendix A (Continued)

constraint 4 // y-

formula: -(x - Pyn1) * Ayn1 - (y - Pyn2) * Ayn2 - (z - Pyn3) * Ayn3 = 0

constraint 5 // z+

formula: -(x - Pzp1) * Azp1 - (y - Pzp2) * Azp2 - (z - Pzp3) * Azp3 = 0

constraint 6 // z-

formula: -(x - Pzn1) * Azn1 - (y - Pzn2) * Azn2 - (z - Pzn3) * Azn3 = 0

constraint 30 nonnegative

formula: z

// Constraints for liquid (calculation)

constraint 7 // keep glue above pad

formula: z = 0

energy:

e1: (-BTENS)

e2: 0

e3: 0

constraint 24 nonnegative // keep glue above substrate

formula: z

constraint 25 nonnegative // keep glue above substrate

formula: z-(Z_LOC-PART_ZDIM/2)

constraint 13 // z- of chip , z+ of glue

formula: -(x - Pzn1) * Azn1 - (y - Pzn2) * Azn2 - (z - Pzn3) * Azn3 = 0

Appendix A (Continued)

energy:

e1: (UPPERT) * (Azn3) * y

e2: (UPPERT) * (Azn1) * z

e3: (UPPERT) * (Azn2) * x

content:

c1: 0

c2:-((Pzn3 + Azn1/Azn3 * Pzn1 + Azn2/Azn3 * (Pzn2 - y)) * x - Azn1/Azn3 * x^2/2)

c3: 0

// One-sided constraints for glue on chip.

constraint 14 nonpositive // keep glue within pos x bound

formula: (x - Pxp1) * Axp1 + (y - Pxp2) * Axp2 + (z - Pxp3) * Axp3

constraint 15 nonpositive // keep glue within neg x bound

formula: (x - Pxn1) * Axn1 + (y - Pxn2) * Axn2 + (z - Pxn3) * Axn3

constraint 16 nonpositive // keep glue within pos y bound

formula: (x - Pyp1) * Ayp1 + (y - Pyp2) * Ayp2 + (z - Pyp3) * Ayp3

constraint 17 nonpositive // keep glue within neg y bound

formula: (x - Pyn1) * Ayn1 + (y - Pyn2) * Ayn2 + (z - Pyn3) * Ayn3

// One-sided constraints for glue on pad.

constraint 19 nonnegative //one-sided x-constraint on pad

formula: x-(0-PAD_XDIM/2)

Appendix A (Continued)

constraint 20 nonpositive //one-sided x-constraint on pad

formula: x-(0+PAD_XDIM/2)

constraint 21 nonnegative //one-sided y-constraint on pad

formula: y-(0-PAD_YDIM/2)

constraint 22 nonpositive //one-sided y-constraint on pad

formula: y-(0+PAD_YDIM/2)

vertices

1 -PAD_XDIM/2 -PAD_YDIM/2 -1e-7 fixed

2 PAD_XDIM/2 -PAD_YDIM/2 -1e-7 fixed

3 PAD_XDIM/2 PAD_YDIM/2 -1e-7 fixed

4 -PAD_XDIM/2 PAD_YDIM/2 -1e-7 fixed

//vertices of plate

5 (X_LOC-PART_XDIM/2) (Y_LOC-PART_YDIM/2) (Z_LOC-PART_ZDIM/2)
constraint 13 14 15 16 17

6 (X_LOC+PART_XDIM/2) (Y_LOC-PART_YDIM/2) (Z_LOC-PART_ZDIM/2)
constraint 13 14 15 16 17

7 (X_LOC+PART_XDIM/2) (Y_LOC+PART_YDIM/2) (Z_LOC-PART_ZDIM/2)
constraint 13 14 15 16 17

8 (X_LOC-PART_XDIM/2) (Y_LOC+PART_YDIM/2) (Z_LOC-PART_ZDIM/2)
constraint 13 14 15 16 17

Appendix A (Continued)

//vertices of Liquid

13 (X_LOC-PART_XDIM/2) (Y_LOC-PART_YDIM/2) 0 constraint 7 19 20 21 22 30

14 (X_LOC+PART_XDIM/2) (Y_LOC-PART_YDIM/2) 0 constraint 7 19 20 21 22 30

15 (X_LOC+PART_XDIM/2) (Y_LOC+PART_YDIM/2) 0 constraint 7 19 20 21 22 30

16 (X_LOC-PART_XDIM/2) (Y_LOC+PART_YDIM/2) 0 constraint 7 19 20 21 22 30

17 (X_LOC-PART_XDIM/2) (Y_LOC-PART_YDIM/2) (Z_LOC-PART_ZDIM/2) constraint 13 14 15 16 17

18 (X_LOC+PART_XDIM/2) (Y_LOC-PART_YDIM/2) (Z_LOC-PART_ZDIM/2) constraint 13 14 15 16 17

19 (X_LOC+PART_XDIM/2) (Y_LOC+PART_YDIM/2) (Z_LOC-PART_ZDIM/2) constraint 13 14 15 16 17

20 (X_LOC-PART_XDIM/2) (Y_LOC+PART_YDIM/2) (Z_LOC-PART_ZDIM/2) constraint 13 14 15 16 17

edges

1 1 2 no_refine fixed

2 2 3 no_refine fixed

3 3 4 no_refine fixed

4 4 1 no_refine fixed

Appendix A (Continued)

5 5 6 constraint 4 6 no_refine

6 6 7 constraint 1 6 no_refine

7 7 8 constraint 3 6 no_refine

8 8 5 constraint 2 6 no_refine

23 13 14 constraint 7 19 20 21 22 30 Aleftq Arightq

24 14 15 constraint 7 19 20 21 22 30 Aleftq Arightq

25 15 16 constraint 7 19 20 21 22 30 Aleftq Arightq

26 16 13 constraint 7 19 20 21 22 30 Aleftq Arightq

27 17 18 constraint 13 17

28 18 19 constraint 13 14

29 19 20 constraint 13 16

30 20 17 constraint 13 15

31 13 17 constraint 30

32 14 18 constraint 30

33 15 19 constraint 30

34 16 20 constraint 30

faces

1 1 2 3 4 fixed no_refine color red

2 5 6 7 8 no_refine tension 0 color green

Appendix A (Continued)

```
14 26 31 -30 -34  constraint 30 tension GAMMA_LV

15 24 33 -28 -32  constraint 30 tension GAMMA_LV

16 23 32 -27 -31  constraint 30 tension GAMMA_LV

17 25 34 -29 -33  constraint 30 tension GAMMA_LV


bodies

1 14 15 16 17 volume 4.7e-8//(PART_XDIM*PART_YDIM*(Z_LOC-PART_ZDIM/2))

read

read "calcplanes.cmd"// normal vector calculations

read "change.cmd" // shift and rotate

read "calcforce.cmd"// calculate forces, torques and hessian

read "xyz.cmd"


target_tolerance := 1e-17 // because of small volume


//new_X_LOC := -40e-6*cos(ti_angle/180*pi); change_X_LOC;

//new_Y_LOC := -40e-6*sin(ti_angle/180*pi); change_Y_LOC;

//ti_CXstep := 20e-6*cos(ti_angle/180*pi);

//ti_CYstep := 20e-6*sin(ti_angle/180*pi);
```

Appendix A (Continued)

```
doinit:=
{
r;g 10;
 r; g10; conj_grad; g10; refine edges where on_constraint 1; g10; g10; }
dostep:=
{
conj_grad on;
g10;
conj_grad off; g 50;
{V;u;V} 4;
g50;
conj_grad on;
g10;
conj_grad off; g50;
}

// g until glue has calmed down
cgl_TOL := 5e-7;
calm_glue :=
{
//printf "cgl: %15.15g -> ",total_energy >> "ti_log.txt";
conj_grad off; g10; conj_grad on;
```

Appendix A (Continued)

```
g20;

do

{

cgl_old_e := total_energy;

g 10;

}

 while (abs((cgl_old_e-total_energy)/total_energy)>cgl_TOL);

//printf "%15.15g -> %15.15g\n",cgl_old_e,total_energy >> "ti_log.txt";

};


Vout:=

{

printf "VLeft %15.15g\n", ((Arightq.value+Aleftq.value<1e-12)?
0.0:(Arightq.value/(Aleftq.value+Arightq.value))*VOLTAGE);

printf "vright %15.15g\n", ((Arightq.value+Aleftq.value<1e-12)?
0.0:(Aleftq.value/(Aleftq.value+Arightq.value))*VOLTAGE);

};
```

Appendix A (Continued)

```
gout:=

{

printf "GLeft %15.15g\n", ((-GAMMA_LV*(cos(angle*pi/180)))-
(((E_o*E_r)/(2*distance))*(((Arightq.value+Aleftq.value)<1e-12)?
0.0:((Arightq.value/(Aleftq.value+Arightq.value))*VOLTAGE)^2)));

printf "Gright %15.15g\n", ((-GAMMA_LV*(cos(angle*pi/180)))-
(((E_o*E_r)/(2*distance))*(((Arightq.value+Aleftq.value)<1e-12)?
0.0:((Aleftq.value/(Aleftq.value+Arightq.value))*VOLTAGE)^2)));

printf "Gsl %15.15g\n", (-GAMMA_LV*cos(angle*pi/180));

};



run_analysis:=

{

doinit;

dostep;

calm_glue;

}



run:=

{

doinit;
```

Appendix A (Continued)

```
dostep;
calm_glue;
forces;
v;
vout;
gout;
}

fz_TOL := 1e-9;
fz_movlim:=0.01e-3;
fz_maxit:=30;
find_zmin := // by Newton-Raphson
{
fz_it :=0;
do
{
fz_it += 1;
fz_old_CZ := Z_LOC;
fz_old_energy := total_energy; // save old values

calc_zf ; // calculate derivative
fz_hstr := dEdz;
```

Appendix A (Continued)

```
fz_alpha := -dEdz/d2Edz2; // Newton


// Apply motion limit
if ( fz_alpha > 0 ) then fz_alpha:=minimum(fz_alpha,fz_movlim)
else fz_alpha:=maximum(fz_alpha,-fz_movlim);


// Shift micropart
new_Z_LOC := fz_old_CZ + fz_alpha;
change_Z_LOC;
calm_glue;


// Backtracking scheme, if Newton failes
if ( total_energy>fz_old_energy) then
{
 fz_alpha := - fz_hstr *fz_alpha^2/(2*(total_energy-fz_hstr*fz_alpha-fz_old_energy));
new_Z_LOC := fz_old_CZ + fz_alpha;
change_Z_LOC; calm_glue;
};
printf "fz %g: Z_LOC: %10e, l: %10e, old_Z_LOC:%10e\n", fz_it
,Z_LOC,fz_alpha,fz_old_CZ >> "ti_log.txt";
} while (abs(fz_old_CZ-Z_LOC)>fz_TOL) and (fz_it<fz_maxit);
};
```